




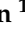


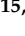


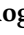





Article

Activation of the Unfolded Protein Response (UPR) Is Associated with Cholangiocellular Injury, Fibrosis and Carcinogenesis in an Experimental Model of Fibropolycystic Liver Disease

Chaobo Chen ^{1,2,3,4,†} , Hanghang Wu ^{1,†}, Hui Ye ^{1,5}, Agustín Tortajada ^{1,2}, Sandra Rodríguez-Perales ⁶, Raúl Torres-Ruiz ⁶, August Vidal ⁷ , María Isabel Peligros ⁸, Johanna Reissing ⁹, Tony Bruns ⁹ , Mohamed Ramadan Mohamed ⁹, Kang Zheng ¹ , Amaia Lujambio ^{10,11,12,13} , María J. Iraburu ¹⁴, Leticia Colyn ¹⁵ , María Ujue Latasa ¹⁵, María Arechederra ^{15,16,17} , Maite G. Fernández-Barrena ^{15,16,17} , Carmen Berasain ^{15,16,17} , Javier Vaquero ^{16,18,19} , Rafael Bañares ^{16,18,19}, Leonard J. Nelson ²⁰ , Christian Trautwein ⁹, Roger J. Davis ²¹ , Eduardo Martínez-Naves ^{1,2}, Yulia A. Nevzorova ^{1,9,16,18}, Alberto Villanueva ⁷ , Matias A. Avila ^{15,16,17,*‡}  and Francisco Javier Cubero ^{1,16,18,*‡} 



Citation: Chen, C.; Wu, H.; Ye, H.; Tortajada, A.; Rodríguez-Perales, S.; Torres-Ruiz, R.; Vidal, A.; Peligros, M.I.; Reissing, J.; Bruns, T.; et al. Activation of the Unfolded Protein Response (UPR) Is Associated with Cholangiocellular Injury, Fibrosis and Carcinogenesis in an Experimental Model of Fibropolycystic Liver Disease. *Cancers* **2022**, *14*, 78. <https://doi.org/10.3390/cancers14010078>

Academic Editor: Edoardo G. Giannini

Received: 2 December 2021

Accepted: 21 December 2021

Published: 24 December 2021

Publisher's Note: MDPI stays neutral with regard to jurisdictional claims in published maps and institutional affiliations.



Copyright: © 2021 by the authors. Licensee MDPI, Basel, Switzerland. This article is an open access article distributed under the terms and conditions of the Creative Commons Attribution (CC BY) license (<https://creativecommons.org/licenses/by/4.0/>).

- ¹ Department of Immunology, Ophthalmology and ENT, Complutense University School of Medicine, 28040 Madrid, Spain; bobo19820106@gmail.com (C.C.); travelerhhang@gmail.com (H.W.); liuchennj@hotmail.com (H.Y.); agustito@ucm.es (A.T.); zhengkang2016@gmail.com (K.Z.); emnaves@med.ucm.es (E.M.-N.); yulianev@ucm.es (Y.A.N.)
- ² 12 de Octubre Health Research Institute (imas12), 28041 Madrid, Spain
- ³ Department of General Surgery, Wuxi Branch of Zhongda Hospital, Southeast University, Wuxi 214105, China
- ⁴ Department of Hepatic-Biliary-Pancreatic Surgery, The Affiliated Drum Tower Hospital of Nanjing University Medical School, Nanjing 210008, China
- ⁵ Department of Anesthesia, Zhongda Hospital, Southeast University, Nanjing 210008, China
- ⁶ Molecular Cytogenetics and Genome Editing Unit, Human Cancer Genetics Program, Centro Nacional de Investigaciones Oncológicas (CNIO), 28029 Madrid, Spain; srodriguezp@cnio.es (S.R.-P.); truirraul27@gmail.com (R.T.-R.)
- ⁷ Laboratorio de Investigación Traslacional (LRT1)-ProCURE, Institut Català d'Oncologia (ICO)-IDIBELL, L'Hospitalet de Llobregat, 08908 Barcelona, Spain; a Vidal@bellvitgehospital.cat (A.V.); avillanueva@iconcologia.net (A.V.)
- ⁸ Institute of Pathology, Hospital Universitario Gregorio Marañón, 28007 Madrid, Spain; isabel.peligros@salud.madrid.org
- ⁹ Department of Internal Medicine III, University Hospital RWTH, 52074 Aachen, Germany; jreissing@ukaachen.de (J.R.); tbruns@ukaachen.de (T.B.); mmohamed@ukaachen.de (M.R.M.); ctrautwein@ukaachen.de (C.T.)
- ¹⁰ Liver Cancer Program, Division of Liver Diseases, Department of Medicine, Tisch Cancer Institute, Icahn School of Medicine at Mount Sinai, New York, NY 10029, USA; amaia.lujambio@mssm.edu
- ¹¹ The Precision Immunology Institute, Icahn School of Medicine at Mount Sinai, New York, NY 10029, USA
- ¹² Graduate School of Biomedical Sciences at Icahn School of Medicine at Mount Sinai, New York, NY 10029, USA
- ¹³ Department of Oncological Sciences, Icahn School of Medicine at Mount Sinai, New York, NY 10029, USA
- ¹⁴ Department of Biochemistry and Genetics, University of Navarra, 31008 Pamplona, Spain; miraburu@unav.es
- ¹⁵ Hepatology Program, Cima, University of Navarra, 31008 Pamplona, Spain; lcolyn@unav.es (L.C.); mulatasa@unav.es (M.U.L.); macalderon@unav.es (M.A.); magarfer@unav.es (M.G.F.-B.); cberasain@unav.es (C.B.)
- ¹⁶ Centro de Investigación Biomédica en Red de Enfermedades Hepáticas y Digestivas (CIBEREHD), Instituto de Salud Carlos III, 28029 Madrid, Spain; javiervaq@hotmail.com (J.V.); rbanares@ucm.es (R.B.)
- ¹⁷ Instituto de Investigaciones Sanitarias de Navarra-IdiSNA, 31008 Pamplona, Spain
- ¹⁸ Instituto de Investigación Sanitaria Gregorio Marañón (IISGM), 28007 Madrid, Spain
- ¹⁹ Servicio de Aparato Digestivo, Hospital General Universitario Gregorio Marañón, 28007 Madrid, Spain
- ²⁰ Institute for Bioengineering (IBioE), Faraday Building, The University of Edinburgh, Edinburgh EH8 9AB, UK; L.Nelson@ed.ac.uk
- ²¹ Howard Hughes Medical Institute, University of Massachusetts Medical School, Worcester, MA 01655, USA; roger.davis@umassmed.edu
- * Correspondence: maavila@unav.es (M.A.A.); fcubero@ucm.es (F.J.C.); Tel.: +34-91-394-1385 (F.J.C.); Fax: +34-91-394-1641 (F.J.C.)
- † These authors contributed equally to this work.
- ‡ These authors contributed equally to this work.

Simple Summary: Polycystic liver disease (PLD) is a group of rare disorders that result from structural changes in the biliary tree development in the liver. In the present work, we studied alterations in molecular mechanisms and signaling pathways that might be responsible for these pathologies. We found that activation of the unfolded protein response, a process that occurs in response to an accumulation of unfolded or misfolded proteins in the lumen of the endoplasmic reticulum, as well as the scarring of the liver tissue, contribute to the pathogenesis of PLD and the development of cancer. As a preclinical animal model we have used mutant mice of a specific signaling pathway, the c-Jun N-terminal kinase 1/2 (*Jnk1/2*). These mice resemble a perfect model for the study of PLD and early cancer development.

Abstract: Fibropolycystic liver disease is characterized by hyperproliferation of the biliary epithelium and the formation of multiple dilated cysts, a process associated with unfolded protein response (UPR). In the present study, we aimed to understand the mechanisms of cyst formation and UPR activation in hepatocytic c-Jun N-terminal kinase 1/2 (*Jnk1/2*) knockout mice. Floxed JNK1/2 (*Jnk^{fl/fl}*) and *Jnk^{Δhepa}* animals were sacrificed at different time points during progression of liver disease. Histological examination of specimens evidenced the presence of collagen fiber deposition, increased α -smooth muscle actin (α SMA), infiltration of CD45, CD11b and F4/80 cells and proinflammatory cytokines (*Tnf*, *Tgf β 1*) and liver injury (e.g., ALT, apoptosis and Ki67-positive cells) in *Jnk^{Δhepa}* compared with *Jnk^{fl/fl}* livers from 32 weeks of age. This was associated with activation of effectors of the UPR, including BiP/GRP78, CHOP and spliced XBP1. Tunicamycin (TM) challenge strongly induced ER stress and fibrosis in *Jnk^{Δhepa}* animals compared with *Jnk^{fl/fl}* littermates. Finally, thioacetamide (TAA) administration to *Jnk^{Δhepa}* mice induced UPR activation, peribiliary fibrosis, liver injury and markers of biliary proliferation and cholangiocarcinoma (CCA). Orthoallografts of DEN/CCl₄-treated *Jnk^{Δhepa}* liver tissue triggered malignant CCA. Altogether, these results suggest that activation of the UPR in conjunction with fibrogenesis might trigger hepatic cystogenesis and early stages of CCA.

Keywords: c-Jun N-terminal kinases (JNK); fibropolycystic liver disease; cholangiocarcinoma (CCA); endoplasmic reticulum (ER) stress; thioacetamide (TAA); CM272

1. Introduction

JNKs are a family of evolutionarily conserved mitogen-activated protein kinases (MAPKs) activated by tumor necrosis factor (TNF) that play an important role in converting extracellular stimuli into a wide range of cellular responses, including inflammatory response, stress response, cell death, cell differentiation and cell proliferation [1,2]. JNKs are encoded by three genes, *Jnk1*, *Jnk2* and *Jnk3*; the products of two of these genes, JNK1 and JNK2, are expressed in the liver [3]. Importantly, JNK1 and JNK2 elicit redundant but also distinct functions [4,5]. In order to characterize the combined functions of the JNK genes, using cell-type-specific deletion models is essential. By implementing this strategy, we were the first to report that aged hepatocyte-specific *Jnk1/2* (*Jnk^{Δhepa}*) knockout mice present bile duct hyperplasia. Moreover, the deletion of *Jnk1/2* in an experimental model of chronic liver disease was strongly associated with cell death, cholestasis and cholangiocyte proliferation [1]. A few months later, Manieri and colleagues [6] reported that changes in bile acid metabolism in *Jnk^{Δhepa}* mice may contribute to cholangiocyte proliferation and hepatoblast maturation, causing bile duct hyperplasia and cholangiocyte injury, which leads to cholangiocarcinoma (CCA) development at late stages. A very recent paper [7] confirmed these findings and identified a molecular link between JNK and RIPK1 as a mechanistic trigger of murine polycystic liver disease (PLD).

PLD is a group of rare disorders that result from structural changes in the biliary tree development [8]. Genetic mechanisms and/or signaling defects are the main cause of ductal structures that become separated from the biliary tree finally resulting in hepatic cystogenesis [9,10]. Cyst formation in the liver may solely affect the intrahepatic bile

ducts (i.e., autosomal dominant polycystic liver disease (ADPLD)) or arise associated with renal cysts [(i.e., autosomal dominant polycystic kidney disease (ADPKD), autosomal recessive polycystic kidney disease (ARPKD), Caroli disease (CD) and CD accompanied by congenital hepatic fibrosis (CHF) in infants, known as Caroli syndrome (CS) [11,12]). Among PLDs, CD patients have an increased risk of developing CCA [13].

The majority of PLD-related genes (i.e., *PRKCSH*, *SEC63*, *ALG8*, *PKD2*, *GANAB*, *SEC61β*) encode for endoplasmic reticulum (ER)-resident proteins involved in the biogenesis, synthesis, maturation, folding and transport of nascent proteins [14]. Therefore, mutations in these genes may compromise ER protein homeostasis, thereby activating the unfolded protein response (UPR) signaling cascades, consisting of sensor (IRE1α, PERK and ATF6) and effector (CHOP, BiP/GRP78 and XBP1) proteins, in order to promote protein folding, ER-associated protein degradation (ERAD) and the activation of prosurvival mechanisms [12].

In the present study, we hypothesized that fibropolycystic-related pathogenesis in *Jnk^{Δhepa}* mice might be triggered concomitantly with the activation of the UPR in response to abnormal ER protein homeostasis thus contributing to uncontrolled cholangiocyte proliferation and cell death.

2. Materials and Methods

2.1. Experimental Models

The generation of hepatocyte-specific *Jnk1/2* knockout mice (*Jnk^{Δhepa}*) in a C57BL/6 background was earlier described [5]. Albumin (Alb)-Cre animals were purchased from Charles River (Cerdanyola del Vallés, Barcelona, Spain). By homologous recombination in embryonic stem (ES) cells, mice with a floxed allele of *Jnk1/2* were constructed *Jnk1/2LoxP/LoxP* (*Jnk^{ff}*) according to previously published studies, and Alb-Cre mice were crossed with *Jnk1/2LoxP/LoxP* to generate *Jnk^{Δhepa}* mice [5,15,16]. Cre-negative *Jnk^{ff}* mice were used as controls.

Age progression of *Jnk^{ff}* and *Jnk^{Δhepa}* mice was followed, and animals were fed until sacrifice at Weeks 8, 32, 52 and 72 of age. Endoplasmic reticulum (ER) stress induction using tunicamycin (TM) liquid solution (Merck, Madrid, Spain) was performed by diluting TM in sterile 150 mM Dextrose with a fixed working concentration. Eight-week-old *Jnk^{ff}* and *Jnk^{Δhepa}* mice received an IP dosage of 2 mg/Kg TM. Control groups received the same IP injection of dextrose solution. Mice were sacrificed 24 h later. Induction of fibrosis in mice was performed using thioacetamide (TAA; Merck, Madrid, Spain) in drinking water (300 mg/L) for a period of 24 weeks to 8-week-old *Jnk^{ff}* and *Jnk^{Δhepa}* mice. Another set of *Jnk^{Δhepa}* male mice received 25 mg/kg (i.p.) of diethyl-nitrosamine (DEN) at 14 days of age and from Week 8 until Week 22 were treated with CCl₄ (0.5 mL/kg, i.p.) twice per week. From Week 18 until Week 22, one group of mice ($n = 6$) was treated with the dual G9a/DNMT1 inhibitor CM272 [17,18] (5 mg/kg, i.p.) daily, while control mice ($n = 6$) received the same volume of PBS. For orthotopic implantation, primary tumors from *Jnk^{ff}* and *Jnk^{Δhepa}*—DEN/CCl₄-treated mice were aseptically isolated and placed at room temperature in DMEM supplemented with 10% FBS plus 50 U/mL penicillin and 50 mg/mL streptomycin and implanted in nude mice, as previously reported [19].

Upon sacrifice, serum was collected from the inferior vena cava, and serum alanine aminotransferase (ALT), aspartate aminotransferase (AST), alkaline phosphatase (AP) and lactate dehydrogenase (LDH) were measured in the Institute of Clinical Chemistry at the University Hospital RWTH Aachen (UKA) using automated analyzers. Liver tissue was collected in liquid nitrogen and kept at -80°C for protein and RNA extraction. A portion was fixed in 4% PFA for immunohistochemistry (IHC) staining and in TissueTek for immunofluorescence (IF) staining.

Both *Jnk^{ff}* mice and *Jnk^{Δhepa}* mice were bred and maintained in the Animal Facility at the School of Biology at UCM, Madrid, under pathogen-free conditions in a temperature and humidity-controlled room with 12 h light/dark cycles and allowed food and water

ad libitum. Animal work was approved by the Consejería de Medio Ambiente, Administración Local y Ordenación del Territorio (PROEX-125.1/20).

2.2. Immunoblot Analysis

According to Bradford's method, protein concentrations in the whole liver tissue lysate, cytoplasm and mitochondria were measured using Bio-Rad protein analysis reagent following the manufacturer's instructions [20]. Immunoblotting was performed as described [1] using the following primary antibodies: BIP/GRP78 (CST, Leiden, Netherlands), CHOP (CST), GAPDH (Bio-Rad, Madrid, Spain), sXBP1 (CST), uXBP1 (Abcam, Cambridge, UK), pJNK1 (BIONOVA, Littleton, CO, USA), JNK1 (CST), pJNK2 (BIONOVA), JNK2 (CST), CK19 (Abcam, Cambridge, UK) and α SMA (Merck). GAPDH was used as a loading control. Primary antibodies were detected with anti-mouse (Bio-Rad) or anti-rabbit (Werfen, Barcelona, Spain) IgG antibodies, and signals were developed using Amersham ECL Prime (GE Healthcare, Madrid, Spain). Quantification of immunoblot signals was performed with the Image Lab Software from Bio-Rad Laboratories. Values were normalized to control signals and are provided together with blot images.

2.3. Histological Evaluation of Samples

Paraffin-embedded hepatic tissue was sectioned and stained for H&E, Periodic Acid Schiff (PAS) and Sirius Red (SR). Samples were examined by a pathologist blinded who analyzed the degree of liver injury. Immunohistochemistry on paraffin sections was performed. Briefly, liver sections were deparaffinized with xylene and rehydrated with serially descending percentages of ethanol. The sections were then boiled in 10 mM sodium citrate acid buffer (pH = 6) to enhance the availability of the antigen, followed by incubation with 3% H₂O₂. Afterward, the sections were transferred to 2.5% horse serum (Palex Medical, Barcelona, Spain) and incubated overnight at 4 °C with CK19 (Abcam), Ki67 (Abcam), SOX9 (Abcam), cleaved caspase-3 (CST), NOTCH1 (Abcam) and MUCIN2 (Santa Cruz, Heidelberg, Germany) antibodies.

The following day, slides were incubated with secondary antibodies (Palex Medical, Madrid, Spain) for 1 h at RT in a humidifying box. The signal was developed with diaminobenzidine (DAB, peroxidase substrate kit) (Palex Medical). The sections were counterstained using hematoxylin and mounted with Roti-Histokit (Quimivita, Barcelona, Spain).

For the immunofluorescence staining, frozen cryosections were incubated with α SMA, Ki67, CD11b (BD Biosciences, Madrid, Spain), CD45 (BD Biosciences) and F4/80 (Bio-Rad) overnight and incubated with fluorescence labeled secondary antibodies (AlexaFluor 488, Fisher Scientific, Madrid, Spain). Slides were then mounted with DAPI (Palex Medical) and imaged using Axio Imager A1 microscope (Carl Zeiss AG, Jena, Germany) and AxioVision software. The cryosections from mouse liver were also incubated with an in situ cell death detection kit (Roche, Madrid, Spain) overnight at 4 °C.

2.4. RNA Isolation and Quantitative Real-Time Polymerase Chain Reaction (RT-PCR)

Total cellular RNA was isolated with Trizol (Fisher Scientific). For reverse transcription, 1 μ g of total RNA was transcribed using Applied Biosystems™ High-Capacity cDNA Reverse Transcription Kit (Fisher Scientific). Quantitative real-time PCR was carried out by a real-time PCR machine employing Sybr Green PCR Master Mix (Fisher Scientific). The Ct values were extrapolated to a standard curve and data was normalized to the house-keeping gene expression (*Gapdh*). Primers' sequences are available upon request.

2.5. Statistical Analysis

All data were expressed as mean \pm standard deviation of the mean. The standard error of the mean (SEM) was calculated from the average of at least 3 independent samples per condition. Statistical significance was determined via using GraphPad Prism 8.0 software (GraphPad Software, CA, USA), followed by a Student's *t*-test (unpaired, two-tailed test)

or via two-way analysis of variance (ANOVA), including Tukey's multiple comparisons test. Values of $p < 0.05$ were considered significant.

3. Results

3.1. Hepatocytic Deletion of *Jnk1/2* Results in Progressive Fibropolycystic Disease Characterized by Extracellular Matrix Deposition and Inflammation

We first generated knockout animals with conditional deletion of both *Jnk1* and *Jnk2* in hepatocytes (*Jnk^{Δhepa}*) (Supplementary Figure S1A,B). Littermates carrying the respective loxP-flanked alleles but lacking expression of Cre recombinase were used as controls (*Jnk^{ff}*) (Supplementary Figure S1A,B). Progression of liver disease was evaluated at 8, 32, 52 and 72 weeks of age (Supplementary Figure S1C).

Interestingly, strong presence of fibrillar collagen networks was identified using Sirius Red (SR) staining in tissue sections from aging *Jnk^{Δhepa}* mice, mimicking CS in patients [7] (Figure 1A). No signs of PKD were observed (Supplementary Figure S2A–C). The quantification of type I and III Collagen fibers in the liver parenchyma of these mice showed a clear tendency from 32 weeks of age and significant differences at 52 and 72 weeks of age, compared to *Jnk^{ff}* mice (Figure 1B). Alpha-smooth muscle actin (α SMA) protein overexpression was evident at 32 weeks of age in *Jnk^{Δhepa}* mice (Figure 1C). Moreover, increased mRNA expression levels of α Sma, *Colla1* and *Mmp9* was observed in aging *Jnk^{Δhepa}* compared with *Jnk^{ff}* livers in most of the time points assessed (Figure 1D).

Synthesis of extracellular matrix (ECM) and activation of myofibroblasts and hepatic stellate cells (HSCs) is often accompanied by the recruitment of leukocytes. Thus, we examined by immunofluorescence (IF) the infiltration of inflammatory cells. The numbers of leukocytes (CD45), macrophages (F4/80) and monocytes (CD11b) were significantly increased in the liver of aging *Jnk^{Δhepa}* mice from 32 weeks of age, compared with *Jnk^{ff}* littermates (Figures 1E and S3A–C). Additionally, the levels of transcripts of proinflammatory cytokines including TNF α and TGF β 1 were significantly elevated in the livers of 32-week-old *Jnk^{Δhepa}* compared with *Jnk^{ff}* mice (Supplementary Figure S3D,E).

3.2. Hepatocytic Deletion of *Jnk1/2* Promotes Hepatomegaly and Liver Damage

Since hepatobiliary pathology manifested by *Jnk^{Δhepa}* mimicked CS to a great extent, we next explored the histological and clinical characteristics of *Jnk^{Δhepa}* aging mice. Hepatomegaly was observed from 52 weeks of age, when mice showed a significantly increased liver weight to body weight (LW/BW) ratio compared with *Jnk^{ff}* animals (Figures 2A and S4A–C). Histologically, from the 52-week-old time point, 100% of *Jnk^{Δhepa}* mice exhibited cysts across the hepatic parenchyma, accompanied by necrotic areas and the presence of inflammatory cells (Figures 2B and S4D).

Next, we measured serum levels of surrogate markers of liver injury in aging *Jnk^{Δhepa}* knockout mice. The biochemical analysis revealed that ALT and LDH levels were significantly increased in *Jnk^{Δhepa}* mice from 52 weeks of age (Figure 2C,D), indicating that hepatocellular injury might be associated with cyst formation observed in *Jnk^{Δhepa}* livers.

Therefore, we subsequently assessed cell death and proliferation using IF and IHC techniques. The TUNEL assay detects DNA breakage that arises during early and late stages of apoptosis [21]. The amount of TUNEL-positive cells per view field was significantly increased in *Jnk^{Δhepa}* livers from 52 weeks of age, compared with *Jnk^{ff}* animals, indicating increased apoptotic cell death in the absence of hepatocytic *Jnk1/2* (Figure 2E). Interestingly, detection of the cleaved form of Caspase-3 (CC3) by IHC was observable already from 32 weeks of age (Supplementary Figure S5A,B). In accordance, a compensatory proliferative response, measured using Ki67-, was evident in *Jnk^{Δhepa}* mice livers, reaching statistical significance from 32 weeks of age when compared with *Jnk^{ff}* mice (Figures 2F and S5C).

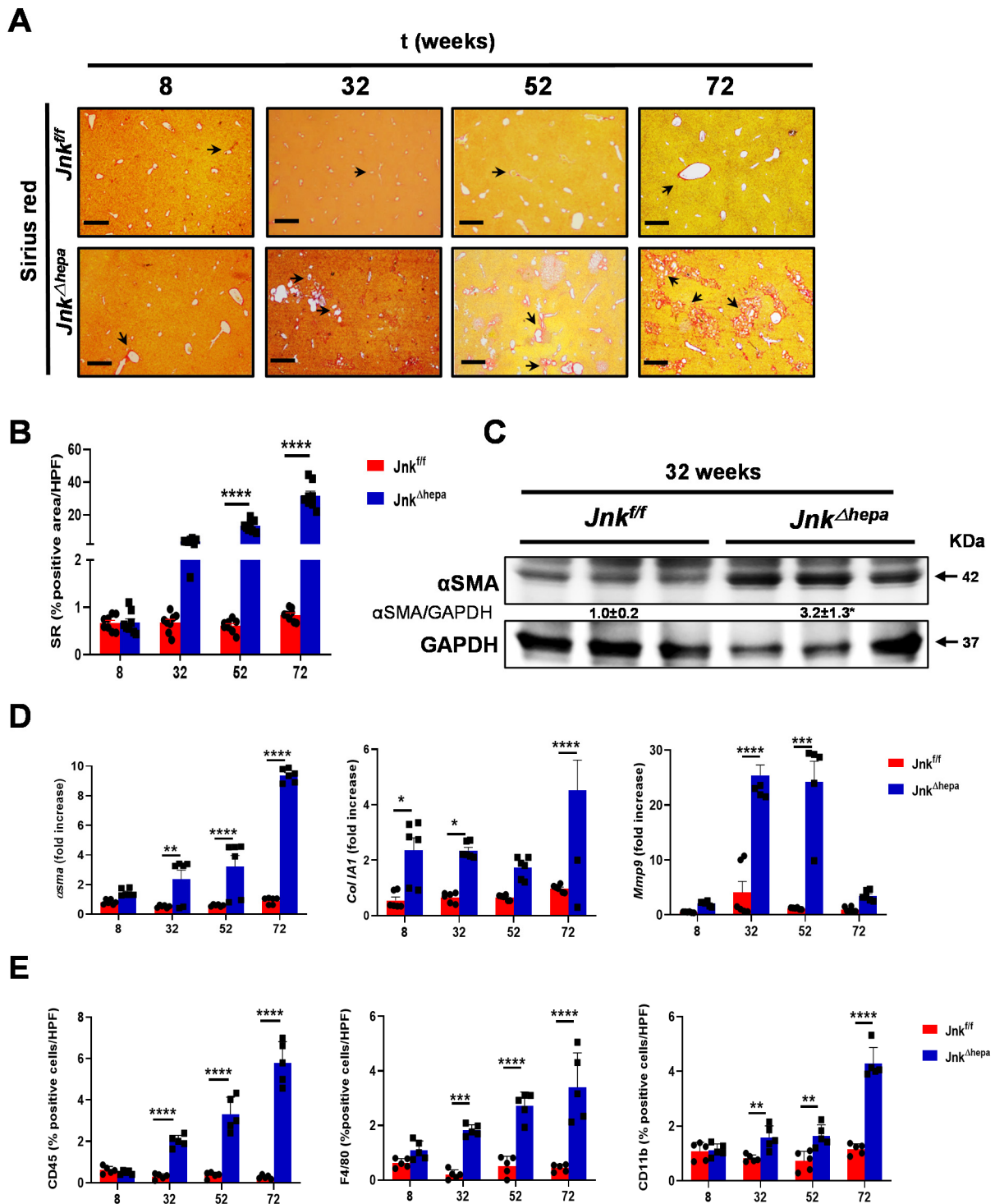


Figure 1. Fibropolycystic disease in aging *Jnk^{Δhepa}* mice is characterized by extracellular matrix deposition and inflammation. (A) Fibrosis was evaluated by SR staining in 8- to 72-week-old *Jnk^{fl/fl}* and *Jnk^{Δhepa}* mice. Scale bars, 500 μm. (B) Quantification of SR areas was performed using ImageJ. Protein and mRNA expression was analyzed for *αSma* (left panel), *Col1A1* (center panel) and *Mmp9* (right panel) using Western Blot (C) and qRT-PCR (D), respectively (* $p < 0.05$; intergroup significance). (E) Quantification of positive cells from IF microphotographs of CD45 (left panel), F4/80 (center panel) and CD11b (right panel) is shown in 8- to 72-week-old *Jnk^{fl/fl}* and *Jnk^{Δhepa}* mice. Data are shown as the mean ± SEM and graphed, separately ($n = 6$ mice per group) (* $p < 0.05$; ** $p < 0.01$; *** $p < 0.001$; **** $p < 0.0001$).

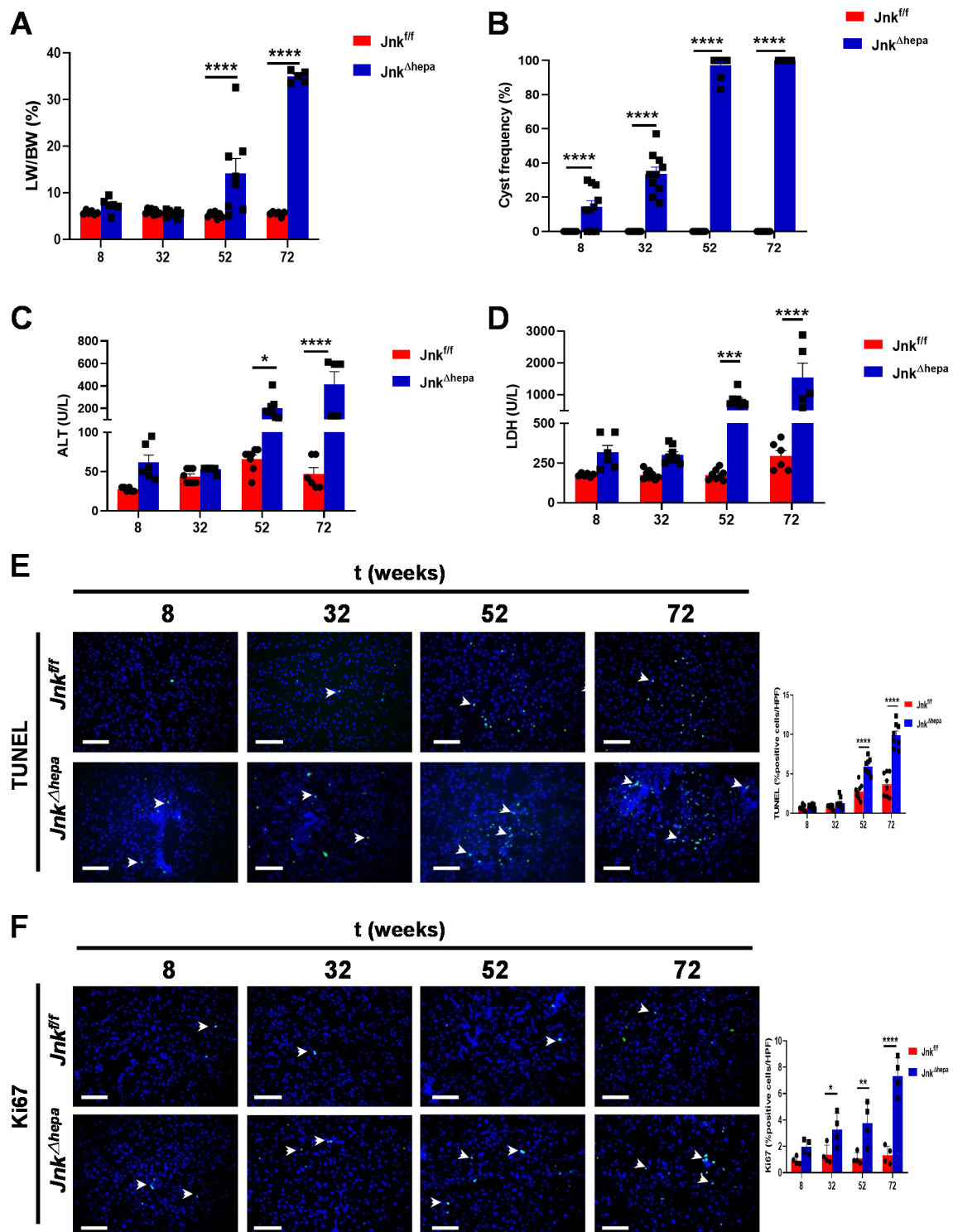


Figure 2. Hepatic deletion of *Jnk1/2* promotes hepatomegaly and liver damage. Eight- to 72-week-old male *Jnk^{fl/fl}* and *Jnk^{Δhepa}* mice were analyzed. (A) Representation of the LW/BW ratio. (B) Liver cysts were counted in the H&E liver tissue staining and represented. Serum ALT (C) and LDH (D) levels were analyzed. (E) Representative microphotographs of TUNEL stainings from *Jnk^{fl/fl}* and *Jnk^{Δhepa}* mice liver tissues collected from 8 to 72 weeks of age and quantification of TUNEL-positive cells/HPF. Scale bars, 50 μ m. (F) Representative microphotographs of Ki67 IF and quantification of Ki67-positive cells/HPF from the same mice. Scale bars, 50 μ m. Data are shown as the mean \pm SEM and graphed, separately ($n = 6$ –8 mice per group) (* $p < 0.05$; ** $p < 0.01$; *** $p < 0.001$; **** $p < 0.0001$).

3.3. Hepatocytic Deletion of *Jnk1/2* Triggers Cystic Hyperproliferation and Cholangiocyte Malignancy

Earlier work demonstrated that hepatocellular JNK deficiency is sufficient for the stimulation of cholangiocyte proliferation and the development of malignancy, resulting in the occurrence of CCA [6]. Therefore, we next studied markers of cystic structures and cholangiocyte proliferation such as CK19 in 52-week-old *Jnk^{fl/fl}* and *Jnk^{Δhepa}* mice. Whereas CK19-positive staining was exclusive of small bile ducts in *Jnk^{fl/fl}* mice, *Jnk^{Δhepa}* livers showed increased staining in cystic areas as a result of massive cholangiocyte proliferation. This was corroborated by significantly elevated CK19 protein and mRNA expression in these livers (Figure 3A,B). Glutamine synthase (GS) is normally expressed around perivenular areas, as in *Jnk^{Δhepa}* livers (Figure 3A, center panel). However, transforming cells express GS. We observed strong positive areas of GS staining are visible in *Jnk^{Δhepa}* livers (Figure 3A, center panel). Concomitant with our GS results, Periodic Acid Schiff (PAS) staining, characteristic of mucin-containing tissues, was restricted to cystic areas in *Jnk^{Δhepa}* livers (Figure 3A, right panel). Next, we analyzed markers of hepatoblast differentiation. Interestingly, the mRNA expression of *Yap1*, a marker of hepatoblast differentiation [22] and *Jag1* and *Hey1*, genes involved in the Notch signaling pathway [23], were significantly upregulated in 52-week-old *Jnk^{Δhepa}* compared with *Jnk^{fl/fl}* mice (Figure 3C–E).

3.4. Activation of the Unfolded Protein Response (UPR) Is Associated with Increased Liver Injury in *Jnk^{Δhepa}* Mice

Hepatic cystogenesis in PLD patients has been recently associated with abnormalities in protein homeostasis in endoplasmic reticulum (ER) [12]. Moreover, severe or prolonged ER stress in epithelial cells is known to result in myofibroblast activation and fibrosis development in different tissues [24]. Therefore, since we detected α SMA overexpression and ECM deposition, indicative of activated myofibroblasts and HSCs, in the livers of *Jnk^{Δhepa}* mice from 32 weeks of age, we analyzed the protein levels of the main UPR components in liver tissue of our experimental groups. Interestingly, while no differences in pIRE α protein expression were observed between *Jnk^{fl/fl}* and *Jnk^{Δhepa}* mice livers (not shown), the UPR effectors BiP/GRP78 and CHOP were strongly overexpressed in 32-week-old *Jnk^{Δhepa}* livers (Figure 4A). These findings were associated with increased levels of spliced and total XBP1 protein levels in *Jnk^{Δhepa}* compared with *Jnk^{fl/fl}* animals (Figure 4A).

Tunicamycin (TM), a bacterial nucleoside that causes accumulation of unfolded or misfolded proteins in the ER, efficiently induces ER stress and activation of the UPR in the liver in vivo [25,26]. Therefore, we used TM as an experimental tool to directly evaluate the effect of UPR activation as a trigger in the fibrogenic response and hepatocellular injury in *Jnk^{Δhepa}* mice. As expected, TM administration resulted in the elevation of UPR effector proteins, including BiP/GRP78, CHOP and XBP1 in *Jnk^{fl/fl}* livers (Figure 4B). However, this response was more intense in *Jnk^{Δhepa}* animals (Figure 4B), indicating increased UPR activation in hepatocytic *Jnk1/2* knockout mice. As indicated by SR staining of liver sections, acute TM dosing triggered a mild fibrogenic response in floxed-control *Jnk^{fl/fl}* mice 24 h after administration. In contrast, this response was much more exacerbated in *Jnk^{Δhepa}* livers (Figures 4C and S6F). Concomitantly, cell death and compensatory proliferation, measured as TUNEL and Ki-67 staining respectively, were significantly increased in the hepatic parenchyma of *Jnk^{Δhepa}* compared with *Jnk^{fl/fl}* animals (Figures 4D,E and S6D,E). Altogether these results show that ER stress and UPR activation are increased in hepatocytic *Jnk1/2* knockout mice, and these animals are much more sensitive to ER-mediated parenchymal damage, explaining the increased fibrosis and hepatocellular injury observed in these mice.

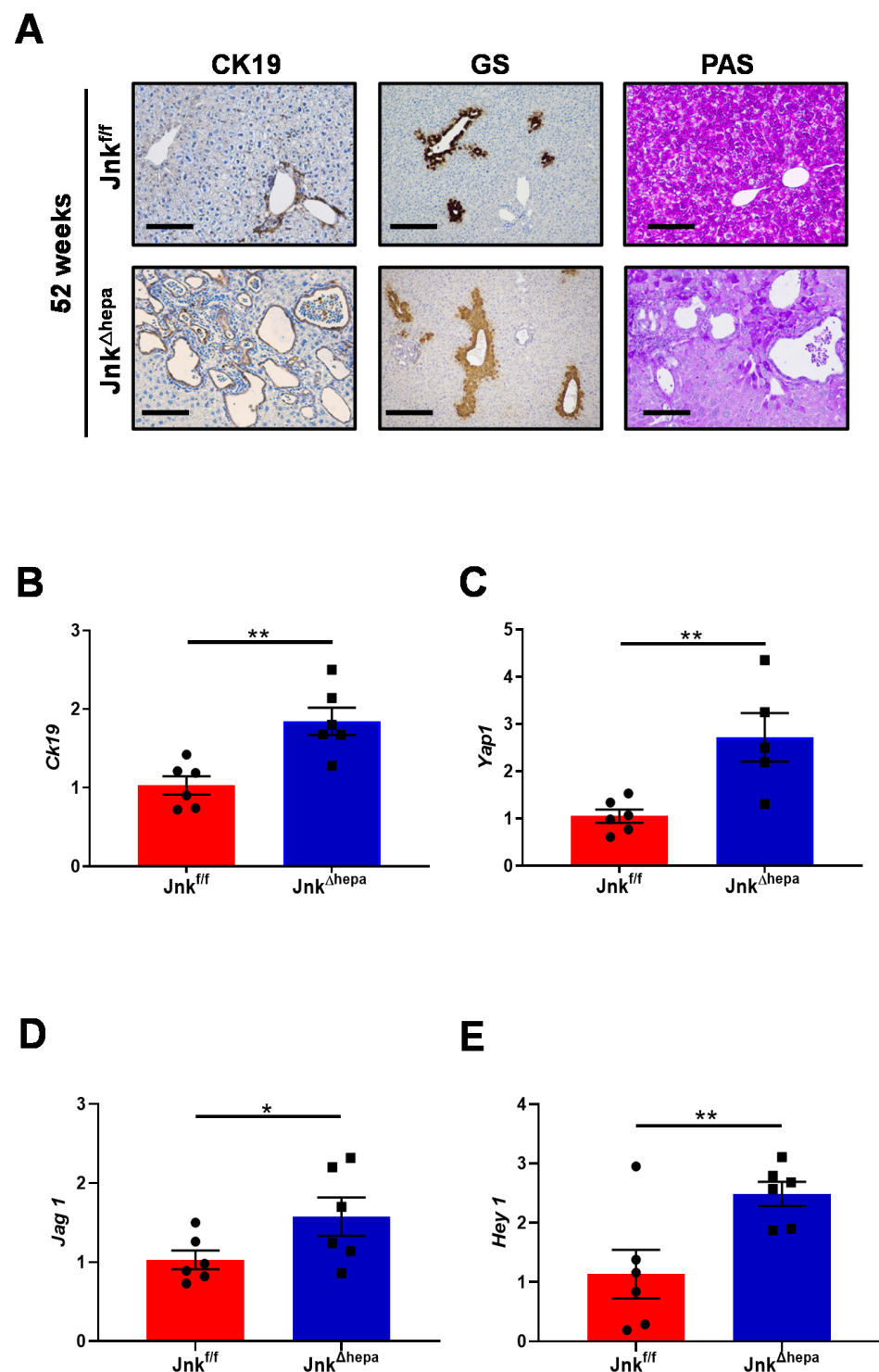


Figure 3. End-stage disease in liver injury of 52-week-old *Jnk^{Δhepa}* mice. (A) Expression of CK19 (left panel), Glutamine synthase (GS) and Periodic Acid Schiff (PAS) were performed in paraffin sections from 52-week-old *Jnk^{ff}* and *Jnk^{Δhepa}* mice livers. Scale bars, 100 μ m. (B–E) Expression of *Ck19*, *Yap1*, *Jag1* and *Hey1* was analyzed and graphed. The data were normalized for the amount of *Gapdh* mRNA in each sample. Data were represented as the mean \pm SEM and graphed, separately ($n = 6$ mice per group, * $p < 0.05$; ** $p < 0.01$).

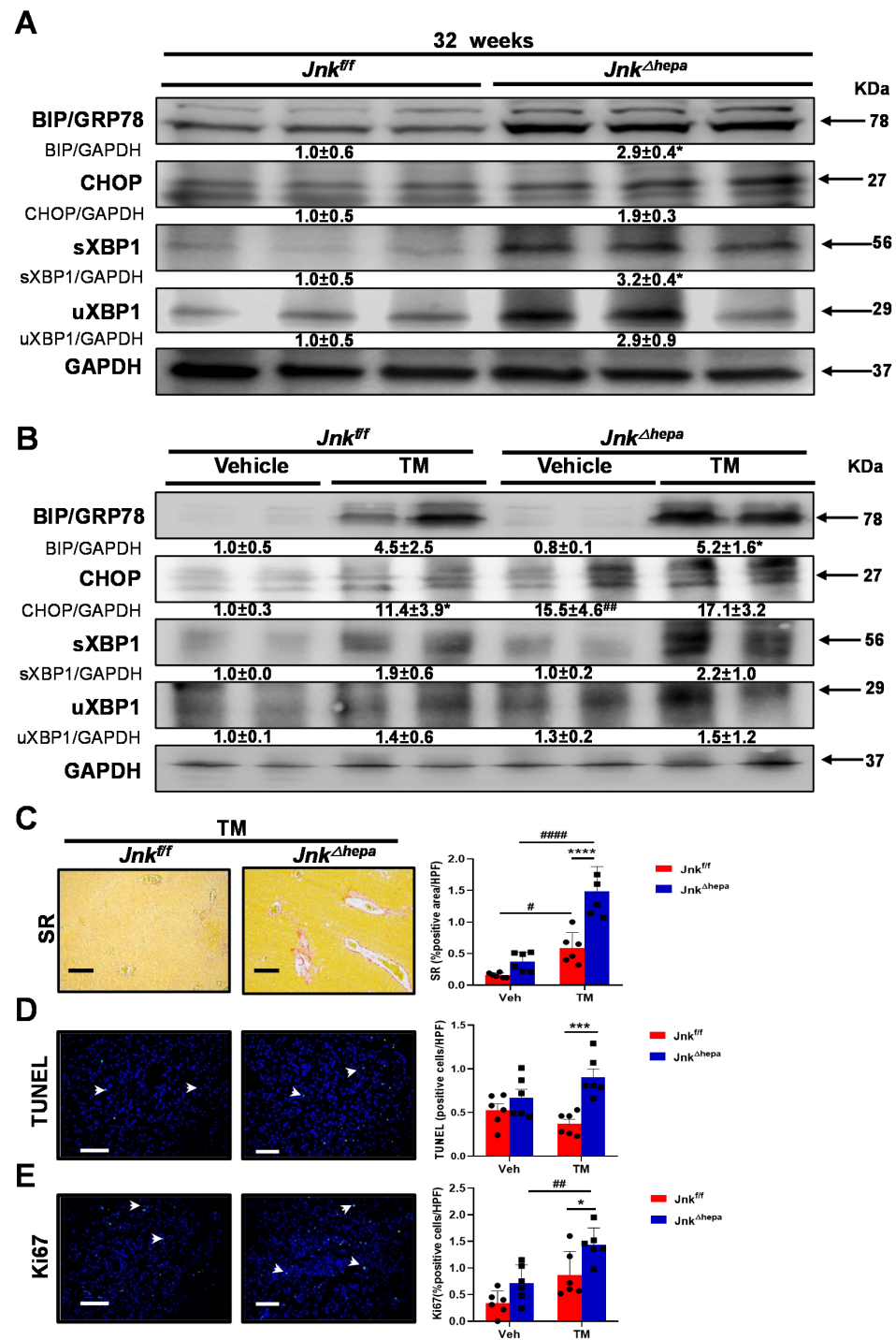


Figure 4. Activation of the unfolded protein response (UPR) triggers increased liver injury in *Jnk^{Δhepa}* mice. (A) The expression of BiP/GRP78, CHOP, spliced XBP1 (sXBP1) and unspliced XBP1 (uXBP1) was evaluated in 32-week-old *Jnk^{fl/fl}* and *Jnk^{Δhepa}* mice using Western blot. (B) The expression of the same proteins was measured in Tunicamycin (TM)-challenged *Jnk^{fl/fl}* and *Jnk^{Δhepa}* mice. Numbers denote molecular weight (KDa) of proteins. GAPDH served as loading control. #/* $p < 0.05$ intra- and intergroup significance, respectively. (C) Representative Sirius Red (SR) stainings of liver tissue from the indicated mice after TM treatment. Scale bars, 500 μ m. (D) TUNEL staining was performed to assess apoptotic cell death in the same samples by IF. Scale bars, 50 μ m. (E) Ki67 was used to measure cell proliferation after TM treatment in the experimental groups. Scale bars, 50 μ m. Data were represented as the mean \pm SEM and graphed ($n = 3-6$ mice per group; /* $p < 0.05$; ## $p < 0.01$; *** $p < 0.001$; ****/#### $p < 0.0001$).

3.5. *Jnk^{Δhepa}* Mice Display an Exacerbated Profibrogenic Response

Since *Jnk^{Δhepa}* mice are more susceptible to ER stress and UPR activation, resulting in an enhanced acute fibrogenic response, we decided to further explore the response of these mice in the context of chronic liver injury. Chronic supplementation in drinking water with thioacetamide (TAA), a toxin known to induce liver injury and cholangiocarcinogenesis in rodents [27] leads to severe fibrosis/cirrhosis between 16 and 24 weeks in mice [28]. Thus, we treated our experimental groups with TAA for a period of 24 weeks (Supplementary Figure S7A). Interestingly, TAA challenge did not result in further induction of UPR effectors except for CHOP expression in *Jnk^{Δhepa}* mice compared with *Jnk^{fl/fl}* littermates (Figure 5A). However, fiber deposition was induced in both experimental groups upon TAA administration, as observed by SR staining (Figure 5B,C). Interestingly, a differential pattern of collagen deposition (SR staining), was observed in the livers of *Jnk^{fl/fl}* and *Jnk^{Δhepa}* mice. While TAA-induced bridging fibrosis in *Jnk^{fl/fl}* livers, the hepatic parenchyma of *Jnk^{Δhepa}* livers displayed peribiliary-like fibrosis (Figure 5B). α SMA levels were evaluated by IF staining and Western blot (Figure 5D,E). Compared with *Jnk^{fl/fl}* mice, activated fibrotic response area was enhanced in *Jnk^{Δhepa}* mice (Figure 5C). Consistently, α SMA protein expression was strongly induced in *Jnk^{Δhepa}* livers, particularly after TAA challenge (Figure 5E). These results suggest that loss of *Jnk1/2* function in hepatocytes promotes exacerbated liver fibrosis.

3.6. *Jnk^{Δhepa}* Mice Display Extensive Hepatocellular Injury in Response to TAA

Given that TAA supplementation caused a strong induction of liver fibrosis in mice with hepatocytic deletion of *Jnk1/2*, we next sought to evaluate the hepatotoxic response to TAA in our experimental groups. TUNEL staining was performed to detect cell death. Microphotographs and data quantification indicated that TAA significantly induced cytotoxicity in both *Jnk^{fl/fl}* and *Jnk^{Δhepa}* animals. However, apoptotic cell death was exacerbated in *Jnk^{Δhepa}* compared with *Jnk^{fl/fl}* livers (Figure 6A,D). Concomitant analysis of cell proliferation using Ki67 indicated that compensatory cell proliferation in response to TAA-induced cell death occurred in both *Jnk^{fl/fl}* and *Jnk^{Δhepa}* animals. Nevertheless, this response was significantly elevated in *Jnk^{Δhepa}* compared with *Jnk^{fl/fl}* livers (Figure 6B,E). Moreover, the frequency of mitotic figures was significantly increased in TAA-treated *Jnk^{Δhepa}* compared with *Jnk^{fl/fl}* livers (Figure 6F).

Histological examination of the livers by H&E staining was performed in both *Jnk^{fl/fl}* and *Jnk^{Δhepa}* livers. Hepatocellular damage and infiltration of inflammatory cells were prominent in TAA-treated *Jnk^{fl/fl}* mice, compared with vehicle-treated animals. Lesion areas in TAA-treated *Jnk^{fl/fl}* mice presented a prominent acinar pattern, combined with cytologic atypia (Figure 6C). However, in *Jnk^{Δhepa}* mice, cells in the lesion area were characterized by strong mitosis accompanied by multiple ductular dilations. At the same time, the ductular dilations and mitotic figures in the lesion areas of TAA-challenged *Jnk^{Δhepa}* mice were significantly different, compared with the structural characteristics of spontaneous cystic dilatations of the ductular tracts in the vehicle-treated group (Figure 6C). Consistently with the enhanced apoptotic and proregenerative (Ki67 labeling) responses found in TAA-treated *Jnk^{Δhepa}* mice, increased circulating levels of ALT, AST, AP and LDH, markers of hepatocellular and biliary injury were detected in these animals (Figure 6G–J).

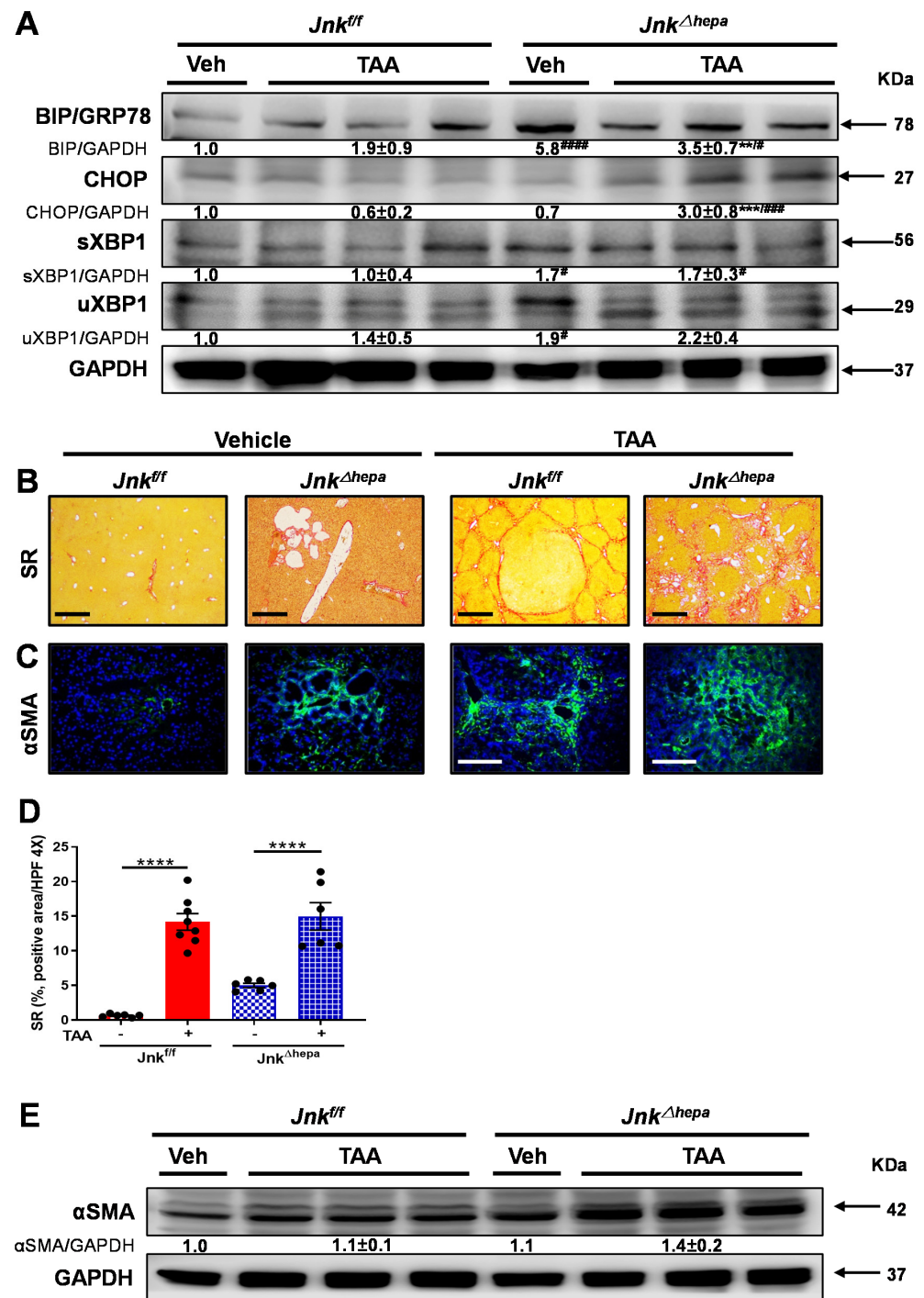


Figure 5. TAA challenge exacerbates liver fibrogenesis in mice with hepatocytic deletion of *Jnk1/2*. (A) The expression of BiP/GRP78, CHOP, spliced XBP1 (sXBP1) and unspliced XBP1 (uXBP1) was evaluated in the livers of *Jnk^{fl/fl}* and *Jnk^{Δhepa}* mice treated or not with TAA using Western blot. Numbers denote molecular weight (KDa) of proteins. GAPDH served as loading control. (B) Representative Sirius Red (SR) stainings of liver paraffin sections from control and TAA-treated *Jnk^{fl/fl}* and *Jnk^{Δhepa}* mice ($n = 6-8$ mice per group). Scale bars, 500 μm . (C) Expression of αSMA protein was assessed via IF staining. Scale bars, 50 μm . (D) Positive area of fibrosis was calculated by ImageJ with microphotographs of SR staining. Data were represented as the mean \pm SEM and graphed. (E) Expression of αSMA was analyzed by Western blot in the indicated groups of mice. Numbers denote molecular weight (KDa) of proteins. GAPDH served as loading control. (# $p < 0.05$; * $p < 0.01$; ***/#### $p < 0.001$; ****/##### $p < 0.0001$).

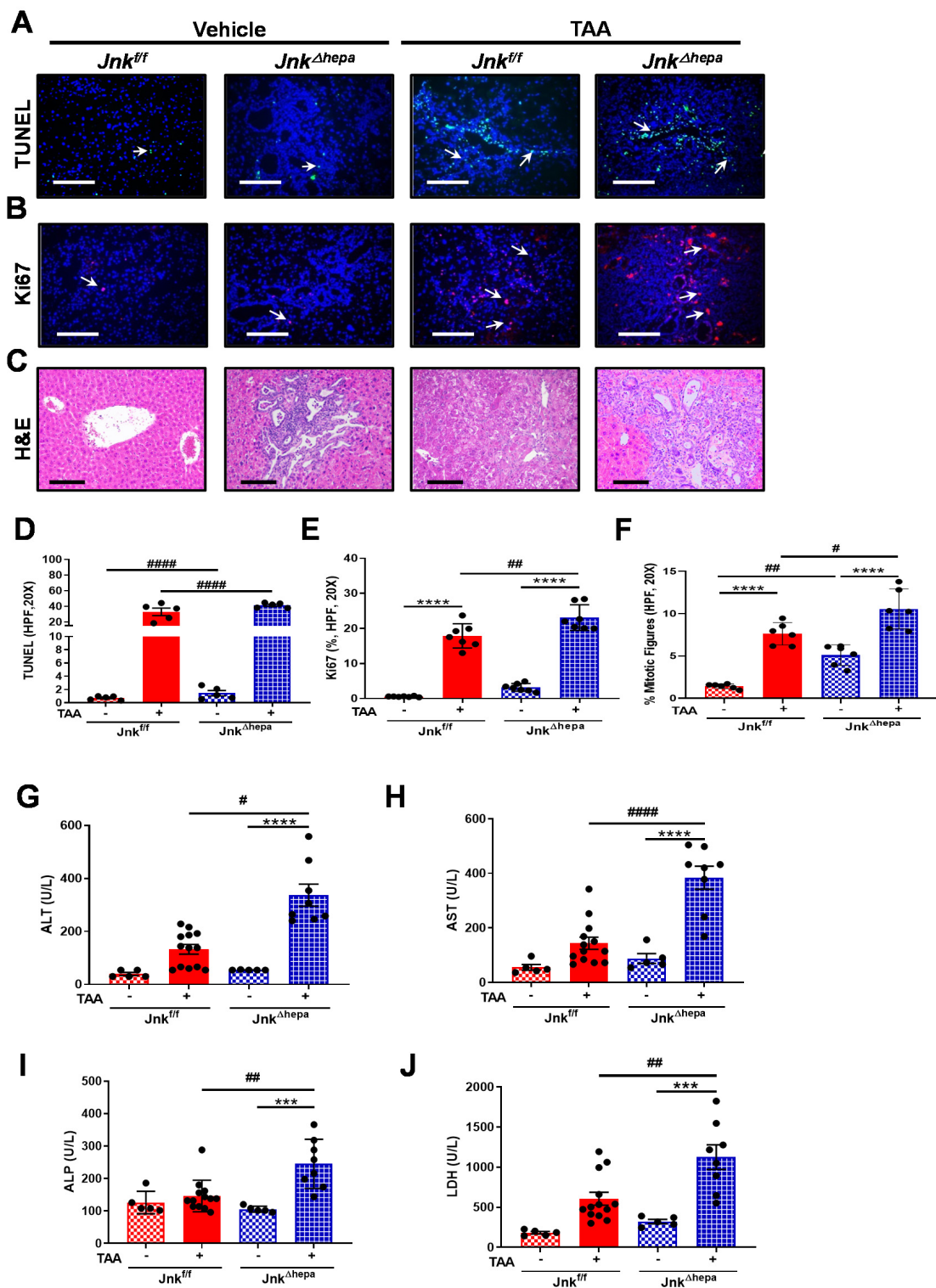


Figure 6. *Jnk^{Δhepa}* mice display extensive hepatocellular and cholangiocellular injury in response to TAA. (A) Cell death was evaluated using TUNEL staining of liver tissue sections from TAA-treated *Jnk^{fl/fl}* and *Jnk^{Δhepa}* mice. Arrows (→) indicate TUNEL positive cells. Scale bars, 50 μm. (B) Expression of Ki67 was evaluated by IF staining. Scale bars, 50 μm. (C) Liver histopathology was analyzed by H&E staining in each experimental group. Positive TUNEL (D), Ki67 cells (E) and frequency of mitotic figures (F) were analyzed by ImageJ and graphed. (G–J) Analysis of serum levels of ALT, AST, ALP and LDH was assessed. Data were represented as the mean ± SEM and graphed (*n* = 5–13 mice per group; # *p* < 0.05; ## *p* < 0.01; *** *p* < 0.001; ****/##### *p* < 0.0001).

3.7. Chronic TAA Administration Triggers Cellular Atypia and Markers of Cholangiocarcinogenesis in $Jnk^{\Delta hepa}$ Mice

As shown above, loss of $Jnk1/2$ in hepatocytes gradually triggers the formation of biliary hamartomas accompanied by the development of ER stress, activation of the UPR, and fibrosis and hepatocellular injury responses, which were enhanced by TAA administration. Since CHF patients have increased risk for CCA [29], we sought to investigate whether carcinogenesis was also enhanced by TAA in our experimental setting. After 24 weeks of TAA administration (Supplementary Figure S7A), no significant differences were observed in the LW/BW ratio between TAA-treated $Jnk^{fl/fl}$ and $Jnk^{\Delta hepa}$ animals (Supplementary Figure S7B–E). However, the number and diameter of nodules observed in the liver surface was significantly higher in $Jnk^{\Delta hepa}$ mice (Supplementary Figure S7F,G).

In view of this, we next evaluated by IHC analysis the expression of typical markers of oval cells and biliary epithelium, including CK19, SOX9, and MUCIN2. While CK19, SOX9 and MUCIN2 were prominent in untreated $Jnk^{\Delta hepa}$ livers, TAA strongly induced their expression compared with $Jnk^{fl/fl}$ animals. Analysis of the mRNA expression of $Yap1$ and $Ck19$ confirmed the enhanced upregulation of biliary proliferation markers [30] induced in the TAA-treated $Jnk^{\Delta hepa}$ mice (Figure 7D,E). Moreover, the percentage of SOX9 and MUCIN2-positive cells per HPF20X were significantly increased in TAA-treated $Jnk^{\Delta hepa}$ compared with $Jnk^{fl/fl}$ mice (Figure 7F,G). Moreover, immunoblotting for CK19 validated the previous observations (Figure 7H). Altogether, markers of cholangiocyte/BECs were strongly activated after treatment with TAA in $Jnk^{\Delta hepa}$ livers.

3.8. Hepatotoxin-Challenged $Jnk^{\Delta hepa}$ Mice Develop Fibrocystic Liver Disease and CCA in Association with a Strong UPR Activation: Therapeutic Potential of an Innovative Epigenetic Inhibitor

So far, our findings reveal that $Jnk^{\Delta hepa}$ mice spontaneously develop hepatic histological and molecular traits indicative of liver injury, fibrosis and a remarkable cystogenesis accompanied by early activation of the UPR. This sequence of events can be accelerated and enhanced by the chronic administration of the hepatotoxin and carcinogen TAA, which also hastens the emergence of markers of CCA development, as seen above. We recently described that when $Jnk^{\Delta hepa}$ mice are treated with a single dose of the carcinogen diethylnitrosamine (DEN), and then chronically challenged with CCl_4 (DEN/ CCl_4 model), instead of hepatocellular carcinomas, these animals develop cyst-like structures with molecular features compatible with cholangioma and malignant CCA [1,17], including upregulated expression of NOTCH1, GS and markers of oval cells ($Ck19$, $Sox9$, $Yap1$ mRNA), as well as increased proliferation measured as $Pcna$ mRNA levels (Supplementary Figure S8A–I), similar to those observed now in response to TAA. In view of this, and of the recognized risk of CCA development in patients with fibrocystic liver diseases, including CD [13,31,32], it was important to provide conclusive evidence of the malignant nature of the lesions developed in these mice. To this end, liver tissue lesions that emerged in $Jnk^{\Delta hepa}$ mice after DEN/ CCl_4 treatment (Supplementary Figure S8A) were resected and orthotopically implanted in nude mice, as previously described [19] (Figure 8A). Mice were followed up and sacrificed 28 weeks after orthoallografts implantation. As shown in Figure 8B, all mice harbored tumoral lesions. Moreover, the engrafted implants displayed histological features resembling those found in TAA and DEN/ CCl_4 treated $Jnk^{\Delta hepa}$ mice livers, compatible with malignant CCA. Histopathological examination revealed that lesions were constituted as glandular and canalicular with cuboidal epithelium and moderate cytologic atypia. All tumors show expansive margins of growth (Figure 8C).

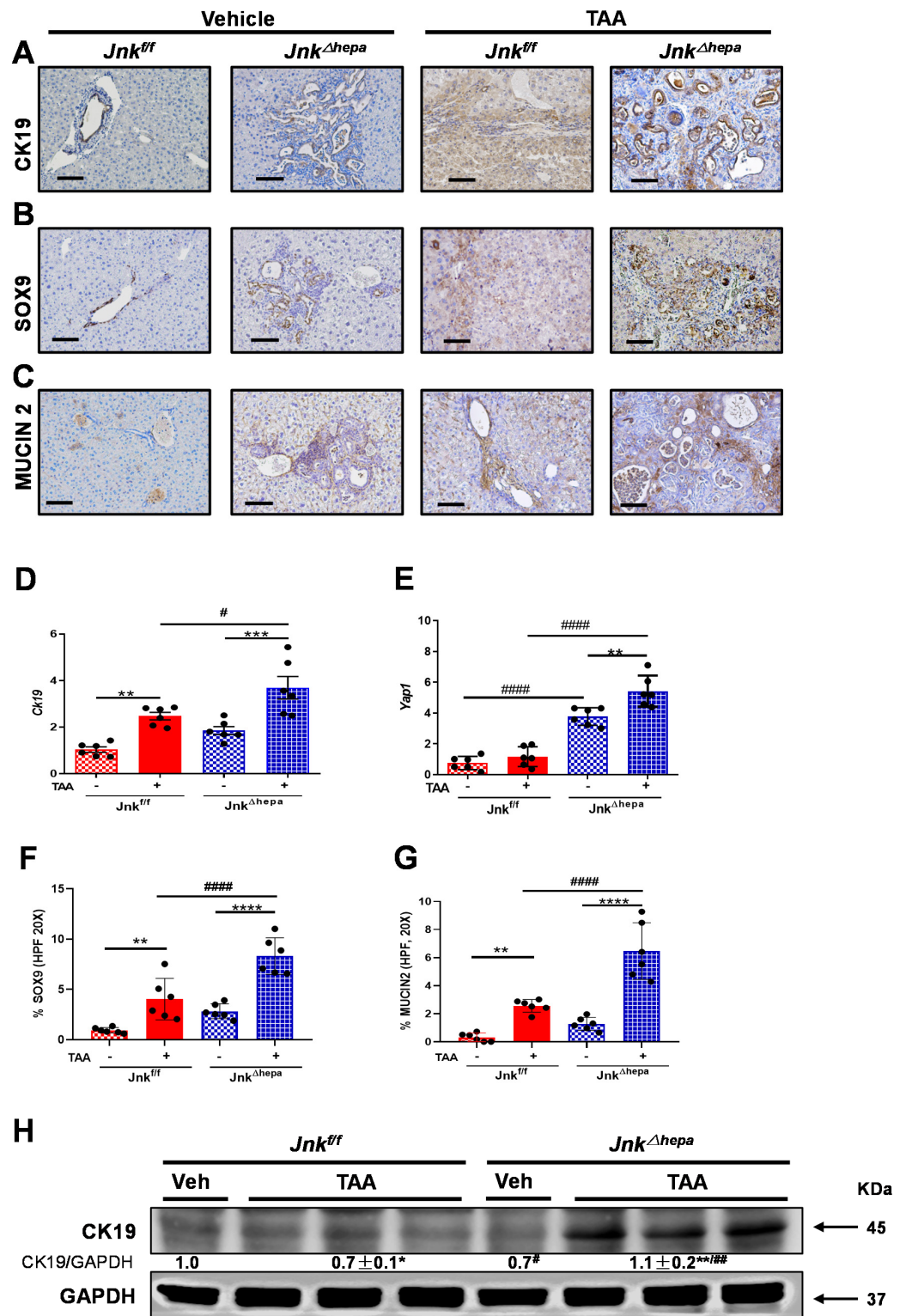


Figure 7. Markers of cholangiocarcinogenesis in *Jnk^{Δhepa}* mice livers upon chronic TAA challenge. (A–C) Representative IHC staining for CK19, SOX9 and MUCIN2. Scale bars, 100 μm. (D,E) mRNA expression of *Yap1* and *Ck19*, was evaluated by qRT-PCR. Quantification of Sox9 and Mucin2 positive cells/HPF (20X) was performed in the same livers. Percentage of SOX9 (F) and MUCIN2 (G) positive cells was performed in HPF (20X) in liver paraffin sections and graphed. (H) Expression of CK19 protein was assessed via Western blot. Numbers denote the molecular weight (KDa) of proteins. GAPDH served as loading control. (*n* = 6; */# *p* < 0.05; **/## *p* < 0.01; *** *p* < 0.001; ****/#### *p* < 0.0001).

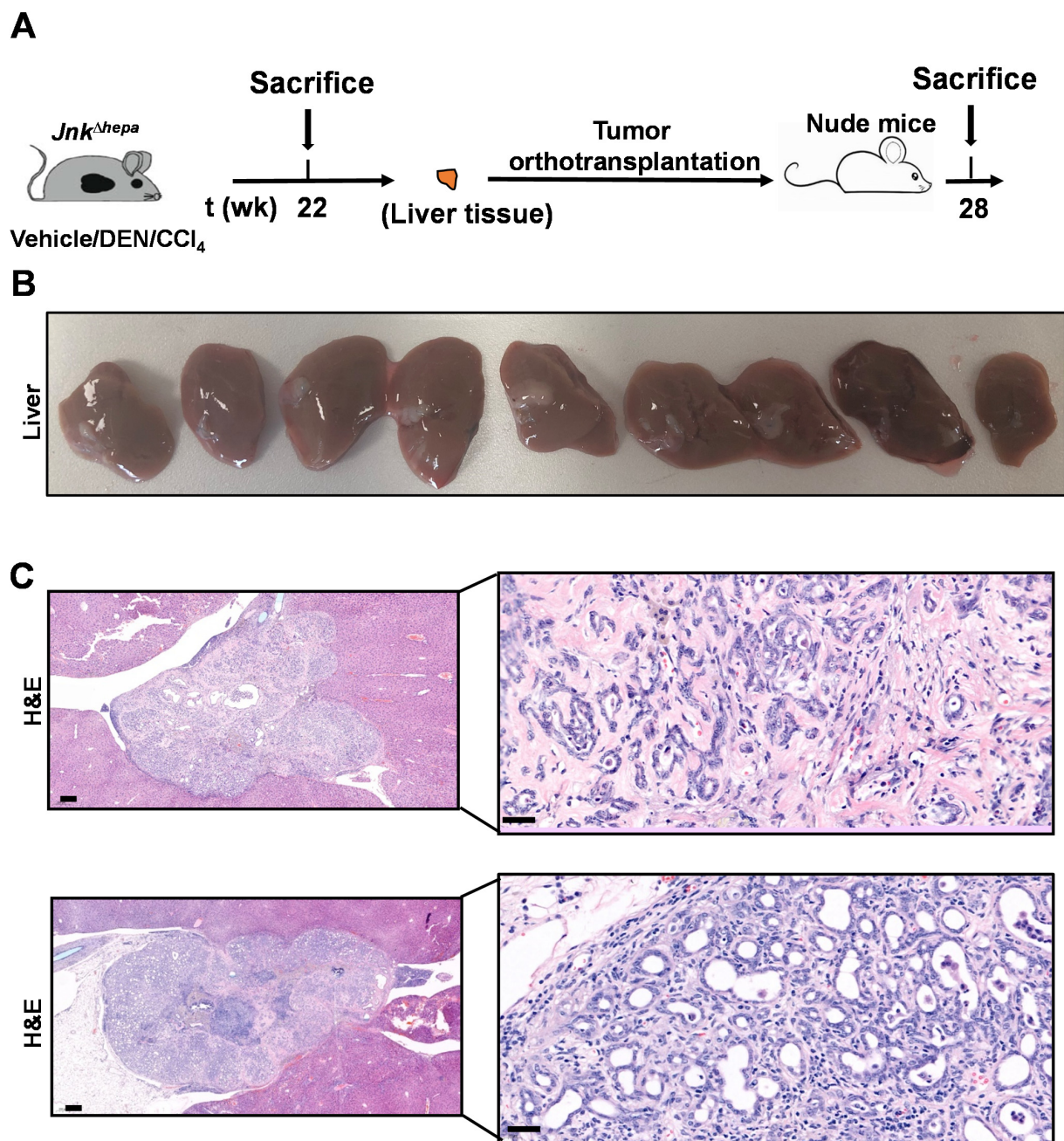


Figure 8. Lesions developed in DEN/CCl₄ treated *Jnk*^{Δhepa} mice are malignant and display CCA histological features. (A) Lesions developed in DEN/CCl₄ treated *Jnk*^{Δhepa} mice were excised and orthotopically implanted in nude mice ($n = 9$), which were sacrificed and analyzed 28 weeks later. (B) Macroscopic aspect of livers from recipient mice after orthotopic implantation of lesions from DEN/CCl₄ treated *Jnk*^{Δhepa} animals. (C) H&E stainings of representative tissue sections of orthoallografts growing in the livers of recipient animals. Scale bars, 50 (left panels) and 200 (right panels) μm , respectively.

We previously showed that by 32 weeks of age, *Jnk*^{Δhepa} mice develop spontaneous liver injury and an UPR (Figures 1, 2 and 4). These features were still not evident in 22-week-old mice (Figure 9A). However, when subjected to the DEN/CCl₄ challenge (as described in Supplementary Figure S8A), 22-week-old *Jnk*^{Δhepa} mice developed strong activation of the UPR (Figure 9B) and a potent cystogenic and fibrogenic response (Figure 9C). We recently described that the malignant progression of CCA-like lesions in DEN/CCl₄ treated *Jnk*^{Δhepa} mice can be inhibited by the administration of CM272, a novel epigenetic drug

that simultaneously targets the histone methyltransferase G9a and DNA-methyltransferase 1 (DNMT1) [17]. Interestingly, CM272 administration, as described in Supplementary Figure S9A, markedly reduced the expression of UPR effectors (Figure 9B) and significantly attenuated the fibrogenic and cystogenic responses (Figure 9C). Most interestingly, CM272 treatment also reduced the levels of NOTCH1 and MUCIN2 and downregulated *Yap1*, *Jag1* and *Hey1* mRNA transcripts, which were induced in the livers of DEN/CCl₄-treated *Jnk^{Δhepa}* mice (Supplementary Figure S9B,C).

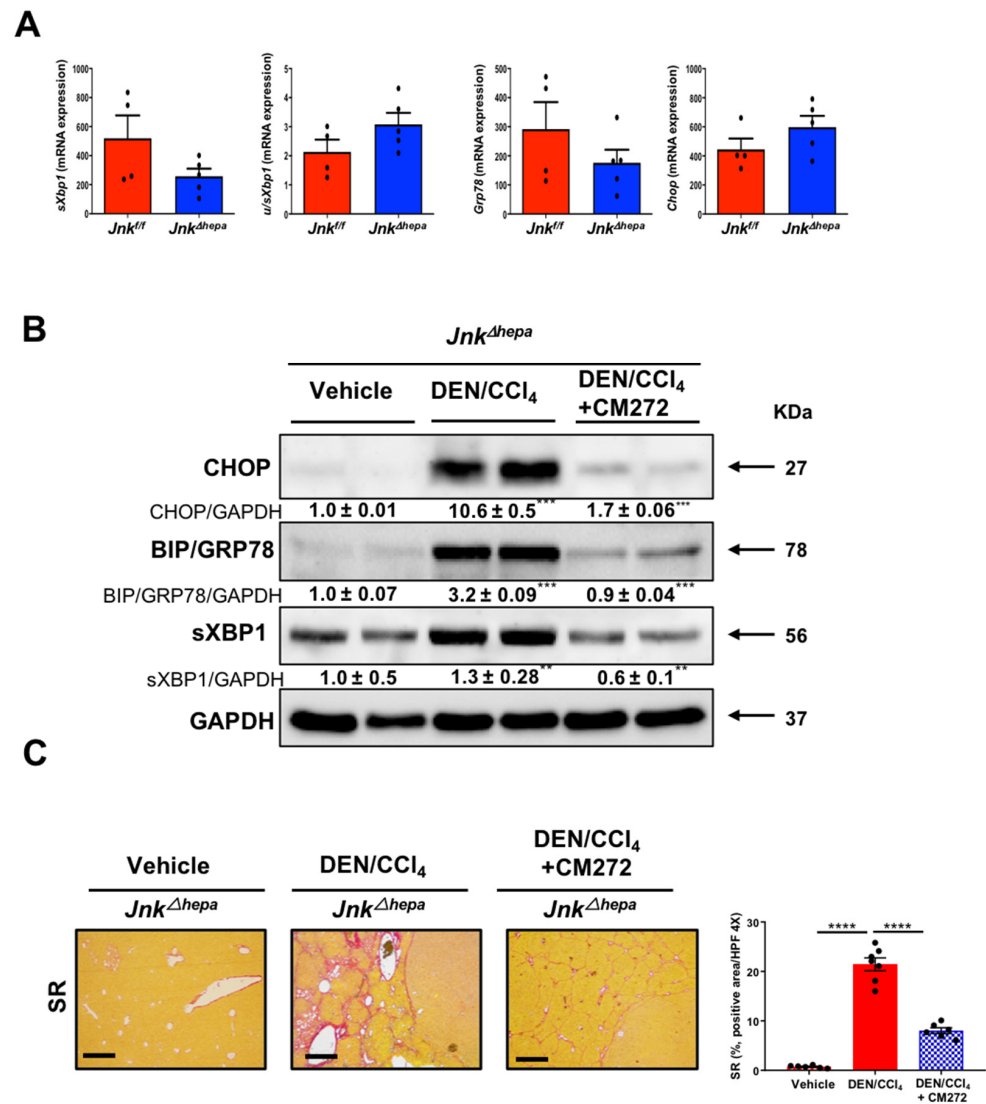


Figure 9. DEN/CCl₄ challenge in *Jnk^{Δhepa}* mice results in the activation of the unfolded protein response (UPR), cystogenesis and fibrosis in the liver: inhibitory effect of targeting the epigenetic G9a/DNMT1 complex. (A) mRNA expression levels of *sXbp1*, *uXbp1*, *Bip/Grp78* and *Chop* evaluated by qRT-PCR in the livers of 22-week-old *Jnk^{fl/fl}* and *Jnk^{Δhepa}* mice. (B) Expression of CHOP, BIP/GRP78 and sXBP1 proteins as assessed by Western blot in *Jnk^{Δhepa}* control mice (Vehicle), DEN/CCl₄-challenged mice and DEN/CCl₄-challenged mice treated with the G9a/DNMT1 inhibitor CM272. Numbers denote the molecular weight (KDa) of proteins. GAPDH served as loading control. Representative images are shown. Bands were quantitated and Vehicle vs. DEN/CCl₄ samples, and DEN/CCl₄ vs. DEN/CCl₄ + CM272 groups were respectively compared. (C) Fibrosis was evaluated by Sirius Red (SR) staining in *Jnk^{Δhepa}* mice treated as indicated. Scale bars, 500 μm. Quantification of SR areas using ImageJ was performed. Data are represented as the mean ± SEM (*n* = 5–7 mice per group, ** *p* < 0.01; *** *p* < 0.001, **** *p* < 0.0001).

4. Discussion

Fibropolycystic disease is an umbrella term that comprises a spectrum of conditions of the intrahepatic bile ducts, characterized by different histological and clinical findings within the liver and other organs.

We were the first to report that mice with disruption of JNK1/2, hepatocyte specific for JNK1, and systemic JNK2 deletion exhibited bile duct hyperplasia at late stages of age progression. Moreover, combined genetic JNK1- and siRNA-JNK2-mediated hepatocyte-specific deletion also caused hepatic cystogenesis [1]. In the present study, we generated *Jnk^{Δhepa}* mice by combining Alb-Cre with *Jnk1Jnk2LoxP* mice. The cyst phenotype has been also observed with the *Alfp-Cre* promoter, revealing that progressive biliary cysts development is independent of the Cre line [7].

Interestingly, our results indicated that the observed phenotype was strongly associated with elevated collagen synthesis and extracellular matrix deposition with activation of HSCs. This is a relevant observation, since patients with Caroli syndrome (CS) present hepatic fibrosis, and therefore, the *Jnk^{Δhepa}* model might be relevant for this relatively understudied disease.

CS is usually diagnosed in early infancy or during childhood, with an estimated incidence rate of 1 in 10,000 to 20,000 live births [33]. Apart from biliary changes, patients with CS exhibit portal fibrosis and inflammation. *Jnk^{Δhepa}* mice from 32 weeks of age and after showed prominent periportal and/or bridging fibrosis, as well as infiltration of immune cells. The phenotype of JNK-hepatocyte knockout mice was characterized by spontaneous liver injury in all 52- and 72-week-old mice. At one year of age, *Jnk^{Δhepa}* animals had significantly increased serum transaminases, LW/BW ratio and exhibited prominent cystogenesis. Moreover, cell death and compensatory proliferation were remarkable in *Jnk^{Δhepa}* mice. However, the nature of cell death remains unclear. In order to understand whether apoptosis or necrosis contributed to biliary proliferation of *Jnk^{Δhepa}* mice, Muller and colleagues [7] additionally deleted Caspase-8, Mkl1 and Ripk1 by creating triple knockout mice. Only deletion of Ripk1 prevented cyst formation. Unfortunately, the interaction and functional relevance of Ripk1 and Jnk in this process need to be further studied. However, in the same study, the authors detected RIPK1 expression in biliary epithelial cells of cystically dilated bile ducts of patients with Caroli disease/syndrome (with additional congenital hepatic fibrosis) [7], suggesting that the regulation of JNK1/RIPK1 signaling could be a potential therapeutic avenue for PLD patients.

Emerging evidence implicates ER stress and UPR signaling in a variety of profibrotic mechanisms in individual cell types. For instance, in epithelial cells, ER stress can induce a profibrotic microenvironment by promoting cell death and activating inflammatory signaling pathways and inducing production of profibrotic mediators that promote fibroblast proliferation and myofibroblast differentiation [24].

The ER is a major intracellular organelle that performs multiple physiological functions including protein folding, post-translational modifications, biosynthesis of fatty acids and sterols, detoxification of xenobiotics, and the storage of intracellular Ca²⁺ [34]. Upon exposure to potential stressors such as drugs, the ER initiates the UPR to restore homeostasis [35]. Specifically important is the ER protein homeostasis, also called proteostasis. A recent publication reported that mutations in genes related to PLD compromise ER proteostasis [12]. While we did not observe changes in sensor proteins of the UPR, including IRE1 or PERK, we observed overexpression of BiP/GRP78 and XBP1 proteins, indicating activation of the UPR effectors in the absence of hepatocytic JNK1/2.

A standard experimental dose of TM (2 mg/kg) induced substantial ER stress in wild-type mice, while robust and exacerbated UPR activation was observed in *Jnk^{Δhepa}* mice after TM challenge, as revealed by overexpression of BiP, CHOP and spliced XBP1, and triggered a fibrogenic response related to cellular injury and compensatory proliferation. To further relate the profibrogenic response to UPR activation and spontaneous liver injury in the absence of hepatocytic JNK1/2, we next challenged *Jnk^{Δhepa}* mice with the profibrotic drug TAA, which causes peribiliary fibrosis [36]. Interestingly TAA administration triggered

a more robust UPR activation in *Jnk^{Δhepa}* animals associated with increased activation of α SMA expression. Moreover, TAA triggered cellular atypia and mitotic figures, as well as centrilobular necrosis in floxed mice. *Jnk^{Δhepa}* animals exhibited strong cholangiocellular injury, as well as significantly altered makers of liver injury.

CS and other ductular plate malformations are known to be risk factors for hepatobiliary neoplasms and more frequently for CCA [37]. Indeed, a recent multicenter study confirmed a CCA rate of 7.3% in a large series of CD and CS patients [32]. Previous work by the group of Sabio [6] reported that changes in bile acid metabolism of *Jnk^{Δhepa}* mice may contribute to cholangiocyte proliferation and hepatoblast maturation, causing bile duct hyperplasia and cholangiocyte injury, which leads to CCA development at late stages. Others did not detect CCA-neoplastic or -dysplastic areas at least at 52 weeks of age [7]. In our hands, progressive expression of markers of hepatoblast differentiation and Notch signaling, which, together with Yap, is a key pathway in cholangiocarcinogenesis [38,39], were detected already in 52-week-old *Jnk^{Δhepa}* mice in the absence of neoplastic lesions on their liver surface. Importantly, nodules were visible in the surface of TAA- and DEN/CCl₄ *Jnk^{Δhepa}*-treated mice livers, as well as the presence of markers of biliary epithelium atypia and cholangiocarcinogenesis, such as the activation of Notch1 and Yap pathways. Malignancy of these tissues was confirmed by orthotopic implantation in athymic NGS mice, also supporting the metastatic potential of the lesions found in chronically injured *Jnk^{Δhepa}* mice livers. These results are in agreement with our previous publication using *NEMO^{Δhepa}* mice [1], altogether indicating that *Jnk^{Δhepa}* livers are sensitive toward CCA development. Interestingly, we also observed that specific inhibition of the epigenetic enzymes G9a and DNMT1, upregulated in human CCA [17] in DEN/CCl₄-challenged *Jnk^{Δhepa}* mice, markedly reduced the activation of the UPR, indicating the attenuation of the ER stress response. Mechanistically, it is unlikely that G9a inhibition directly results in the abolition of ER stress, as the level of H3K9me3, the chromatin repressive mark to which G9a contributes, is reduced on the promoters of *Chop* and *BiP/Grp78* genes concomitant with their upregulation during ethanol-induced chronic liver injury and ER stress in mice [40]. Inflammatory mediators play a central role in triggering ER stress and the UPR in liver injury and chronic liver diseases [41]. The strong anti-inflammatory effect mediated by G9a/DNMT1 inhibition that we previously described in DEN/CCl₄ *Jnk^{Δhepa}* mice and other mouse models of chronic liver injury [17,42] might contribute to explain the attenuation of the UPR by CM272 treatment found in the present study. Noteworthy, here, we also observed that CM272 treatment concomitantly reduced the activation of the Notch pathway. This response is consistent with the stimulatory effect of G9a on Notch signaling previously described in endothelial precursor cells [43]. Notch inhibition, together with a potent TGF β antagonism as we reported [42], may underlie the therapeutic effects of CM272 on liver fibrocystic disease and carcinogenic progression [31,44]. Nevertheless, the detailed mechanisms of CM272-mediated inhibition of the Notch pathway need to be further explored.

5. Conclusions

Our study links ER stress and fibrosis with cholangiocellular injury and cell death in *Jnk^{Δhepa}* mice, which are sensitive to CCA development. Therefore, the *Jnk^{Δhepa}* model can be a relevant experimental tool for the study of fibropolycystic liver diseases including CS. Our work also identifies potential therapeutic strategies for a group of diseases lacking effective medical treatments.

Supplementary Materials: The following supporting information can be downloaded at: <https://www.mdpi.com/article/10.3390/cancers14010078/s1>. Figure S1. (A) Genotyping for *Jnk1* and *Jnk2*. Ethidium Bromide gel showed the respective PCR results from mice tails DNA derived from *Jnk^{Δhepa}* mice. (B) Immunoblot analysis to demonstrate the deletion of *JNK1* and *JNK2*. *GAPDH* was used as a loading control. (C) Experimental setting: *Jnk^{f/f}* and *Jnk^{Δhepa}* mice were sacrificed at different time points of the progression of liver disease, 8, 32, 52 and 72 weeks. Figure S2. (A) Macroscopic view of the kidney of ageing *Jnk^{f/f}* and *Jnk^{Δhepa}* mice. (B) H&E staining was performed

in the kidneys of 8 to 72-week-old Jnkf/f and JnkΔhepa mice. Scale bars, 200 μm. (C) Sirius Red (SR) staining was performed in the kidneys of 8 to 72-week-old Jnkf/f and JnkΔhepa mice. Scale bars, 100 μm. Figure S3. (A) Representative IF microphotographs of 8 to 72 week-old Jnkf/f and JnkΔhepa mice for CD45 (B), F4/80 (C), CD11b (D). Scale bar, 200 μm. The mRNA expression of Tnf (E) and Tgfβ1 (F) was calculated and graphed in 32 week-old Jnkf/f and JnkΔhepa mice (*** $p < 0.001$, **** $p < 0.0001$). Figure S4. Liver weight, LW (A) and body weight, BW (B) were measured in ageing Jnkf/f and JnkΔhepa mice (mean ± SEM; $n = 6-8$ per time point; ** $p < 0.01$, *** $p < 0.001$, **** $p < 0.0001$). (C) Macroscopic view of livers from ageing Jnkf/f and JnkΔhepa mice at 8, 32, 52 and 72 weeks of age. (D) H&E staining was performed in paraffin sections of the same livers. Figure S5. (A) Immunohistochemistry staining for cleaved caspase 3 (CC3) was performed in liver sections of ageing Jnkf/f and JnkΔhepa mice, from 8 to 72 weeks of age. (B) Quantification of positive cells was measured and graphed ($n = 6-8$, ** $p < 0.01$, *** $p < 0.001$, **** $p < 0.0001$). (C) Immunohistochemistry staining for Ki67 was performed in liver sections of ageing Jnkf/f and JnkΔhepa mice, from 8 to 72 weeks of age. Figure S6. (A) Sirius Red (SR) was performed for 8 week-old vehicle-treated Jnkf/f and JnkΔhepa mice and microphotographs are shown. (B) TUNEL was assessed for the same mice and a microphotograph is shown. (C) Ki67 was performed in the same samples and a microphotograph is shown. Figure S7. (A) Eight week-old Jnkf/f and JnkΔhepa male mice were used for administration of TAA in drinking water (300mg/L). Mice were sacrificed 24 weeks later ($n = 6-13$). (B) Macroscopic pictures of the liver after sacrifice are shown. BW (C), LW (D) and LW/BW (E) ratio was calculated. (F) Total liver nodules were counted and represented after treatment. (G) Diameter of liver nodules was measured and graphed. Data are shown as mean ± SEM and graphed (* $p < 0.05$; ** $p < 0.01$, *** $p < 0.001$; intragroup and # $p < 0.05$ intergroup comparison). Figure S8. (A) Seven week-old Jnkf/f and JnkΔhepa male mice were used for administration of DEN/CCl4. Mice were sacrificed 8 weeks after DEN injection ($n = 7$). Notch1 (B), Glutamine synthase (GS) (C) and PCNA (D) immunohistochemistry staining were performed in liver paraffin sections of these animals. mRNA expression of PCNA (E), Ck19 (F), Sox9 (H) and Yap1 (I) was analyzed and graphed. The data were normalized for the amount of GAPDH mRNA in each sample. Data are shown as mean ± SEM and graphed (****/##### $p < 0.001$; ***/### $p < 0.001$). Figure S9. (A) Schematic representation of the animal model used. (B) Notch1 and Mucin-2 immunohistochemistry staining were performed in liver paraffin sections of these animals. Scale bars, 500 μm. (C) Expression of Yap1, Hey1 and Jag1 was analyzed and graphed. The data were normalized for the amount of GAPDH mRNA in each sample. Data are shown as the mean SEM ($n = 5$ mice per group; ** $p < 0.01$; **** $p < 0.0001$).

Author Contributions: Data curation, C.C., H.W., H.Y.; Formal analysis, C.C., H.W., H.Y., M.J.I., L.C., M.U.L., M.G.F.-B., J.V.; Methodology, investigation, A.T., S.R.-P., R.T.-R., A.V. (August Vidal), M.I.P., J.R., T.B., M.R.M., K.Z., A.L., J.V., R.J.D., E.M.-N., Y.A.N., A.V. (Alberto Villanueva), M.A.A., F.J.C.; Visualization, A.V. (Alberto Villanueva), M.I.P., J.R., T.B., M.R.M., M.J.I., L.C., M.U.L., M.A., M.G.F.-B.; Writing—original draft, writing—review and editing, M.A.A., F.J.C.; Funding acquisition, project administration, E.M.-N., Y.A.N., M.A.A., F.J.C.; Supervision, validation, C.B., R.B., L.J.N., C.T., R.J.D., E.M.-N., Y.A.N., A.V. (Alberto Villanueva), M.A.A., F.J.C. All authors have read and agreed to the published version of the manuscript.

Funding: This research was funded by the MINECO Retos PID2020-117941RB-IOO, SAF2016-78711 and SAF2017-87919-R, MINECO Retos PID2019-104878RB-100AEI/10.13039/501100011033, EXOHEP-CM S2017/BMD-3727, NanoLiver-CM Y2018/NMT-4949, ERAB Ref. EA 18/14, AMMF 2018/117, UCM-25-2019, the German Research Foundation (SFB/TRR57/P04, SFB 1382-403224013/A02 and DFG NE 2128/2-1), and COST Action CA17112. T.B. was supported by the German Research Foundation (DFG) (SFB1382 Project ID 403114013/B07). C.C. is supported with a scientific research project of Wuxi Municipal Health Commission (M202160). L.J.N. is a recipient of a BBSRC (Grant BB/L023687/1) and a EPSRC (IAA Grant PIII013) grants. Y.A.N., M.G.F.B and F.J.C. are Ramón y Cajal Researcher RYC-2015-17438, RYC-2018-024475-1 and RYC-2014-15242, respectively. M.A. is a postdoctoral fellow of the Asociación Española Contra el Cáncer (AECC). L.C. is a predoctoral fellow of the Gobierno de Navarra. CT was supported by the German Research Foundation (DFG CRC1382 #403224013, TR285/10-2, GRK 2375). F.J.C. is a Gilead Liver Researcher 2018. The research group belongs to the validated Research Groups Ref. 970935 Liver Pathophysiology, 920631 Lymphocyte immunobiology, 920361 “Inmunogenética e inmunología de las mucosas” and IBL-6 (imas12-associated).

Institutional Review Board Statement: The animal study protocol was approved by the Consejería de Medio Ambiente, Administración Local y Ordenación del Territorio (PROEX-125.1/20).

Informed Consent Statement: Not applicable.

Data Availability Statement: The data presented in this study are available in this article (and supplementary material).

Conflicts of Interest: The funders had no role in the design of the study; in the collection, analyses, or interpretation of data; in the writing of the manuscript, or in the decision to publish the results.

References

1. Cubero, F.J.; Mohamed, M.R.; Woitok, M.M.; Zhao, G.; Hatting, M.; Nevzorova, Y.A.; Chen, C.; Haybaeck, J.; de Bruin, A.; Avila, M.A.; et al. Loss of c-jun n-terminal kinase 1 and 2 function in liver epithelial cells triggers biliary hyperproliferation resembling cholangiocarcinoma. *Hepatol. Commun.* **2020**, *4*, 834–851. [[CrossRef](#)] [[PubMed](#)]
2. Sabio, G.; Davis, R.J. Tnf and map kinase signalling pathways. *Semin. Immunol.* **2014**, *26*, 237–245. [[CrossRef](#)] [[PubMed](#)]
3. Seki, E.; Brenner, D.A.; Karin, M. A liver full of jnk: Signaling in regulation of cell function and disease pathogenesis, and clinical approaches. *Gastroenterology* **2012**, *143*, 307–320. [[CrossRef](#)] [[PubMed](#)]
4. Davis, R.J. Signal transduction by the jnk group of map kinases. *Cell* **2000**, *103*, 239–252. [[CrossRef](#)]
5. Cubero, F.J.; Zoubek, M.E.; Hu, W.; Peng, J.; Zhao, G.; Nevzorova, Y.A.; Al Masaoudi, M.; Bechmann, L.P.; Boeschoten, M.V.; Muller, M.; et al. Combined activities of jnk1 and jnk2 in hepatocytes protect against toxic liver injury. *Gastroenterology* **2016**, *150*, 968–981. [[CrossRef](#)]
6. Manieri, E.; Folgueira, C.; Rodriguez, M.E.; Leiva-Vega, L.; Esteban-Lafuente, L.; Chen, C.; Cubero, F.J.; Barrett, T.; Cavanagh-Kyros, J.; Seruggia, D.; et al. Jnk-mediated disruption of bile acid homeostasis promotes intrahepatic cholangiocarcinoma. *Proc. Natl. Acad. Sci. USA* **2020**, *117*, 16492–16499. [[CrossRef](#)]
7. Muller, K.; Honcharova-Biletska, H.; Koppe, C.; Egger, M.; Chan, L.K.; Schneider, A.T.; Kusgens, L.; Bohm, F.; Boege, Y.; Healy, M.E.; et al. Jnk signaling prevents biliary cyst formation through a caspase-8-dependent function of ripk1 during aging. *Proc. Natl. Acad. Sci. USA* **2021**, *118*, e2007194118. [[CrossRef](#)]
8. Cnossen, W.R.; Drenth, J.P. Polycystic liver disease: An overview of pathogenesis, clinical manifestations and management. *Orphanet J. Rare Dis.* **2014**, *9*, 69. [[CrossRef](#)]
9. Drenth, J.P.; Christijjn, M.; Bergmann, C. Congenital fibrocystic liver diseases. *Best Pract. Res. Clin. Gastroenterol.* **2010**, *24*, 573–584. [[CrossRef](#)]
10. Strazzabosco, M.; Fabris, L. Development of the bile ducts: Essentials for the clinical hepatologist. *J. Hepatol.* **2012**, *56*, 1159–1170. [[CrossRef](#)]
11. Perugorria, M.J.; Banales, J.M. Genetics: Novel causative genes for polycystic liver disease. *Nat. Rev. Gastroenterol. Hepatol.* **2017**, *14*, 391–392. [[CrossRef](#)]
12. Santos-Laso, A.; Izquierdo-Sanchez, L.; Rodrigues, P.M.; Huang, B.Q.; Azkargorta, M.; Lapitz, A.; Munoz-Garrido, P.; Arbelaz, A.; Caballero-Camino, F.J.; Fernandez-Barrena, M.G.; et al. Proteostasis disturbances and endoplasmic reticulum stress contribute to polycystic liver disease: New therapeutic targets. *Liver Int.* **2020**, *40*, 1670–1685. [[CrossRef](#)]
13. Strazzabosco, M.; Somlo, S. Polycystic liver diseases: Congenital disorders of cholangiocyte signaling. *Gastroenterology* **2011**, *140*, 1855–1859.e1. [[CrossRef](#)] [[PubMed](#)]
14. Lee-Law, P.Y.; Olaizola, P.; Caballero-Camino, F.J.; Izquierdo-Sanchez, L.; Rodrigues, P.M.; Santos-Laso, A.; Azkargorta, M.; Elortza, F.; Martinez-Chantar, M.L.; Perugorria, M.J.; et al. Targeting ubc9-mediated protein hyper-sumoylation in cystic cholangiocytes halts polycystic liver disease in experimental models. *J. Hepatol.* **2021**, *74*, 394–406. [[CrossRef](#)] [[PubMed](#)]
15. Das, M.; Jiang, F.; Sluss, H.K.; Zhang, C.; Shokat, K.M.; Flavell, R.A.; Davis, R.J. Suppression of p53-dependent senescence by the jnk signal transduction pathway. *Proc. Natl. Acad. Sci. USA* **2007**, *104*, 15759–15764. [[CrossRef](#)] [[PubMed](#)]
16. Das, M.; Sabio, G.; Jiang, F.; Rincon, M.; Flavell, R.A.; Davis, R.J. Induction of hepatitis by jnk-mediated expression of tnf-alpha. *Cell* **2009**, *136*, 249–260. [[CrossRef](#)]
17. Colyn, L.; Barcena-Varela, M.; Alvarez-Sola, G.; Latasa, M.U.; Uriarte, I.; Santamaria, E.; Herranz, J.M.; Santos-Laso, A.; Arechederra, M.; Ruiz de Gauna, M.; et al. Dual targeting of g9a and DNA methyltransferase-1 for the treatment of experimental cholangiocarcinoma. *Hepatology* **2021**, *73*, 2380–2396. [[CrossRef](#)]
18. San Jose-Eneriz, E.; Agirre, X.; Rabal, O.; Vilas-Zornoza, A.; Sanchez-Arias, J.A.; Miranda, E.; Ugarte, A.; Roa, S.; Paiva, B.; Estella-Hermoso de Mendoza, A.; et al. Discovery of first-in-class reversible dual small molecule inhibitors against g9a and dnmts in hematological malignancies. *Nat. Commun.* **2017**, *8*, 15424. [[CrossRef](#)]
19. Ambrogio, C.; Carmona, F.J.; Vidal, A.; Falcone, M.; Nieto, P.; Romero, O.A.; Puertas, S.; Vizoso, M.; Nadal, E.; Poggio, T.; et al. Modeling lung cancer evolution and preclinical response by orthotopic mouse allografts. *Cancer Res.* **2014**, *74*, 5978–5988. [[CrossRef](#)]
20. An, L.; Wang, X.; Cederbaum, A.I. Cytokines in alcoholic liver disease. *Arch. Toxicol.* **2012**, *86*, 1337–1348. [[CrossRef](#)]
21. Mirzayans, R.; Murray, D. Do tunnel and other apoptosis assays detect cell death in preclinical studies? *Int. J. Mol. Sci.* **2020**, *21*, 9090. [[CrossRef](#)]

22. Lee, D.H.; Park, J.O.; Kim, T.S.; Kim, S.K.; Kim, T.H.; Kim, M.C.; Park, G.S.; Kim, J.H.; Kuninaka, S.; Olson, E.N.; et al. Lats-yap/taz controls lineage specification by regulating *tgfbeta* signaling and *hnf4alpha* expression during liver development. *Nat. Commun.* **2016**, *7*, 11961. [[CrossRef](#)]
23. Fischer, A.; Schumacher, N.; Maier, M.; Sendtner, M.; Gessler, M. The notch target genes *hey1* and *hey2* are required for embryonic vascular development. *Genes Dev.* **2004**, *18*, 901–911. [[CrossRef](#)]
24. Kropski, J.A.; Blackwell, T.S. Endoplasmic reticulum stress in the pathogenesis of fibrotic disease. *J. Clin. Investig.* **2018**, *128*, 64–73. [[CrossRef](#)] [[PubMed](#)]
25. Marciniak, S.J.; Yun, C.Y.; Oyadomari, S.; Novoa, I.; Zhang, Y.; Jungreis, R.; Nagata, K.; Harding, H.P.; Ron, D. Chop induces death by promoting protein synthesis and oxidation in the stressed endoplasmic reticulum. *Genes Dev.* **2004**, *18*, 3066–3077. [[CrossRef](#)] [[PubMed](#)]
26. Zhang, K.; Shen, X.; Wu, J.; Sakaki, K.; Saunders, T.; Rutkowski, D.T.; Back, S.H.; Kaufman, R.J. Endoplasmic reticulum stress activates cleavage of *crebh* to induce a systemic inflammatory response. *Cell* **2006**, *124*, 587–599. [[CrossRef](#)] [[PubMed](#)]
27. Dwyer, B.J.; Jarman, E.J.; Gogoi-Tiwari, J.; Ferreira-Gonzalez, S.; Boulter, L.; Guest, R.V.; Kendall, T.J.; Kurian, D.; Kilpatrick, A.M.; Robson, A.J.; et al. Tweak/*fn14* signalling promotes cholangiocarcinoma niche formation and progression. *J. Hepatol.* **2021**, *74*, 860–872. [[CrossRef](#)] [[PubMed](#)]
28. Delire, B.; Starkel, P.; Leclercq, I. Animal models for fibrotic liver diseases: What we have, what we need, and what is under development. *J. Clin. Transl. Hepatol.* **2015**, *3*, 53–66. [[PubMed](#)]
29. Khan, S.A.; Tavolari, S.; Brandi, G. Cholangiocarcinoma: Epidemiology and risk factors. *Liver Int.* **2019**, *39* (Suppl. S1), 19–31. [[CrossRef](#)] [[PubMed](#)]
30. Gadd, V.L.; Aleksieva, N.; Forbes, S.J. Epithelial plasticity during liver injury and regeneration. *Cell Stem Cell* **2020**, *27*, 557–573. [[CrossRef](#)] [[PubMed](#)]
31. Lasagni, A.; Cadamuro, M.; Morana, G.; Fabris, L.; Strazzabosco, M. Fibrocystic liver disease: Novel concepts and translational perspectives. *Transl. Gastroenterol. Hepatol.* **2021**, *6*, 26. [[CrossRef](#)]
32. Fard-Aghaie, M.H.; Makridis, G.; Reese, T.; Feyerabend, B.; Wagner, K.C.; Schnitzbauer, A.; Bechstein, W.O.; Oldhafer, F.; Kleine, M.; Klempnauer, J.; et al. The rate of cholangiocarcinoma in caroli disease a german multicenter study. *HPB* **2021**, in press. [[CrossRef](#)]
33. Chen, I.Y.; Whitney-Miller, C.L.; Liao, X. Congenital hepatic fibrosis and its mimics: A clinicopathologic study of 19 cases at a single institution. *Diagn. Pathol.* **2021**, *16*, 81. [[CrossRef](#)]
34. Hur, K.Y.; So, J.S.; Ruda, V.; Frank-Kamenetsky, M.; Fitzgerald, K.; Koteliansky, V.; Iwawaki, T.; Glimcher, L.H.; Lee, A.H. *Irelalpha* activation protects mice against acetaminophen-induced hepatotoxicity. *J. Exp. Med.* **2012**, *209*, 307–318. [[CrossRef](#)]
35. Ron, D.; Walter, P. Signal integration in the endoplasmic reticulum unfolded protein response. *Nat. Rev. Mol. Cell Biol.* **2007**, *8*, 519–529. [[CrossRef](#)] [[PubMed](#)]
36. Nevzorova, Y.A.; Boyer-Diaz, Z.; Cubero, F.J.; Gracia-Sancho, J. Animal models for liver disease—A practical approach for translational research. *J. Hepatol.* **2020**, *73*, 423–440. [[CrossRef](#)] [[PubMed](#)]
37. Choe, J.Y.; Kim, H. Intrahepatic cholangiocarcinoma with predominant ductal plate malformation pattern. *Clin. Mol. Hepatol.* **2014**, *20*, 214–217. [[CrossRef](#)] [[PubMed](#)]
38. Lu, X.; Peng, B.; Chen, G.; Pes, M.G.; Ribback, S.; Ament, C.; Xu, H.; Pal, R.; Rodrigues, P.M.; Banales, J.M.; et al. Yap accelerates notch-driven cholangiocarcinogenesis via *mtorc1* in mice. *Am. J. Pathol.* **2021**, *191*, 1651–1667. [[CrossRef](#)] [[PubMed](#)]
39. Wang, H.; Song, X.; Liao, H.; Wang, P.; Zhang, Y.; Che, L.; Zhang, J.; Zhou, Y.; Cigliano, A.; Ament, C.; et al. Overexpression of mothers against decapentaplegic homolog 7 activates the yes-associated protein/notch cascade and promotes liver carcinogenesis in mice and humans. *Hepatology* **2021**, *74*, 248–263. [[CrossRef](#)]
40. Esfandiari, F.; Medici, V.; Wong, D.H.; Jose, S.; Dolatshahi, M.; Quinlivan, E.; Dayal, S.; Lentz, S.R.; Tsukamoto, H.; Zhang, Y.H.; et al. Epigenetic regulation of hepatic endoplasmic reticulum stress pathways in the ethanol-fed cystathionine beta synthase-deficient mouse. *Hepatology* **2010**, *51*, 932–941. [[CrossRef](#)]
41. Duvigneau, J.C.; Luis, A.; Gorman, A.M.; Samali, A.; Kaltenecker, D.; Moriggl, R.; Kozlov, A.V. Crosstalk between inflammatory mediators and endoplasmic reticulum stress in liver diseases. *Cytokine* **2019**, *124*, 154577. [[CrossRef](#)] [[PubMed](#)]
42. Barcena-Varela, M.; Paish, H.; Alvarez, L.; Uriarte, I.; Latasa, M.U.; Santamaria, E.; Recalde, M.; Garate, M.; Claveria, A.; Colyn, L.; et al. Epigenetic mechanisms and metabolic reprogramming in fibrogenesis: Dual targeting of *g9a* and *dnmt1* for the inhibition of liver fibrosis. *Gut* **2021**, *70*, 388–400. [[CrossRef](#)] [[PubMed](#)]
43. Chi, L.; Ahmed, A.; Roy, A.R.; Vuong, S.; Cahill, L.S.; Caporiccio, L.; Sled, J.G.; Caniggia, I.; Wilson, M.D.; Delgado-Olguin, P. *G9a* controls placental vascular maturation by activating the notch pathway. *Development* **2017**, *144*, 1976–1987. [[CrossRef](#)]
44. Fabris, L.; Fiorotto, R.; Spirli, C.; Cadamuro, M.; Mariotti, V.; Perugorria, M.J.; Banales, J.M.; Strazzabosco, M. Pathobiology of inherited biliary diseases: A roadmap to understand acquired liver diseases. *Nat. Rev. Gastroenterol. Hepatol.* **2019**, *16*, 497–511. [[CrossRef](#)] [[PubMed](#)]